Pre-print version: Pulatsu, B., Gonen, S., Erdogmus, E., Lourenço, P.B., Lemos, J.V., and Prakash R., "*In-Plane Structural Performance of Dry-Joint Stone Masonry Walls A Spatial and Non-Spatial Stochastic Discontinuum Analysis*.", Engineering Structures (2021). **DOI**: 10.1016/j.engstruct.2021.112620

In-Plane Structural Performance of Dry-Joint Stone Masonry Walls: A Spatial and Non-Spatial Stochastic Discontinuum Analysis

Bora Pulatsu[a,*], Semih Gonen[b], Ece Erdogmus[a], Paulo B. Lourenço[c], Jose V. Lemos[d] and Ravi Prakash[e]

Abstract: In this study, the in-plane structural behavior, capacity, and performance of dry-joint stone masonry walls (DJ- SMWs) and the effects of the vertical stress level on these factors are investigated via a stochastic discontinuum analysis that considers the material uncertainty. A discontinuum type of analysis is performed based on the discrete element method (DEM), where each stone masonry unit is explicitly represented in the computational model. To better simulate the cracking and shear failure modes within the stone units, a coupled fracture energy- based contact constitutive model is implemented into a commercial discrete element code, 3DEC. First, the proposed modeling approach is validated by comparing to experimental findings in literature. Then, the approach is used to explore the failure mechanism and the force–displacement behavior of DJ-SMWs, considering different vertical stress levels and material properties. The results of the novel modeling strategy provide a better understanding of the progressive collapse mechanism of DJ-SMWs and the influence of the vertical stress level. Furthermore, the outcomes of this research indicate the major role of the frictional resistance at the joints in the safety and performance assessment of the dry-joint load-bearing masonry walls. Finally, important inferences are made regarding the non-spatial and spatial stochastic discontinuum analysis.

Keywords: DEM; Dry-joint masonry wall; Contact mechanics; Material uncertainty; Stochastic analysis; Uncertainty quantification

[a] Carleton University, Civil and Environmental Engineering, Ottawa, ON, Canada
[b] Oslo Metropolitan University, Department of Civil Engineering and Energy Technology, Oslo, Norway
[c] Institute of Sustainability and Innovation in Structural Engineering, University of Minho, Portugal
[d] LNEC, Lisbon, Portugal
[e] Indian Institute of Technology Jodhpur, India

* Corresponding author: bora.pulatsu@carleton.ca

Pre-print version: Pulatsu, B., Gonen, S., Erdogmus, E., Lourenço, P.B., Lemos, J.V., and Prakash R., "*In-Plane Structural Performance of Dry-Joint Stone Masonry Walls A Spatial and Non-Spatial Stochastic Discontinuum Analysis*.", Engineering Structures (2021). **DOI**: 10.1016/j.engstruct.2021.112620

1 Introduction

Unreinforced masonry (URM) is the most used ancient construction technique, dating back thousands of years due to its inherent durability. Generally, URM structures are built with local materials and made up of masonry units (such as stone, clay brick, or adobe) laid dry or bonded with mortar. In this research, special attention is given to the safety assessment of ***unreinforced dry-joint stone masonry walls*** (DJ-SMWs). The DJ-SMWs serve as the main load bearing structural element for many ancient constructions, existing stone-built cultural heritage, and residential buildings. DJ-SMWs can be composed of regular cut stones or built in a disordered (irregular) configuration, where the structural stability predominantly depends on the frictional resistance among the stone interfaces. Furthermore, even when there is mortar between the units, weathering effects and lack of maintenance cause significant deterioration and often the total loss of the mortar, or at least of the loss of mortar-stone bond, over the lifetime of a structure, eventually rendering it similar to a dry-joint system. Recent and past earthquakes demonstrated that many of the unreinforced dry-joint and low-bond strength masonry structures are vulnerable to seismic actions and have been severely affected by past earthquakes [1–3]. Therefore, to better preserve, repair, and strengthen these structures, a thorough understanding of the DJ-SMW behavior under combined compression-shear forces is necessary.

Even though the seismic assessment of stone architectural heritage has drawn a growing interest over the last decades, a limited number of experimental data are available in the literature. The joint properties of such masonry type have been recently examined to gain a better insight into the initial and residual frictional resistance at the joints [4,5]. Furthermore, large scale tests have been performed to investigate the macro behavior of DJ-SMWs under monotonic and cyclic loading [6,7]. Wang et al. [8] tested the effectiveness of different retrofitting applications using local materials to increase the lateral capacity of DJ-SMWs subjected to cyclic loading. Velez et al. [9] performed a series of quasi-static tilting table tests on reduced scale dry-joint masonry structures with different configurations (e.g., walls and one- and two-story houses) to obtain their out-of-plane failure mechanisms and capacity (or collapse multiplier).

Besides, different computational modeling approaches have been proposed to simulate DJ-SMWs, based on finite and/or discrete element methods. Lourenço et al. [6] and Senthivel and

Lourenço [10] carried out two-dimensional (2D) discontinuous nonlinear finite element analysis (FEA), referred to as micro-modeling, to predict the force-displacement response of DJ-SWMs, considering plane stress continuum elements for stone units and zero thickness line interface elements for the joints. A similar approach, so called finite-discrete element method (FDEM), was applied to simulate various dry-joint stone masonry constructions in two- and three-dimensions by Smoljanovic et al. [11,12]. In FDEM, the simulation of fracture in the stone masonry walls is achieved using embedded pre-defined contact elements implemented within the triangular (2D) or tetrahedral (3D) finite elements. Ngapeya et al. [13] investigated the influence of the geometrical imperfections on the load-bearing capacity of dry-joint hollow concrete masonry walls, where link elements (working in compression but not in tension) were utilized in nonlinear FEA analysis. Moreover, alternative simple equilibrium models (based on strut-and-tie representation) were proposed by Roca [14] to predict the ultimate capacity of URM shear walls. Recently, Bui et al. [15] studied the in-plane and out-of-plane behavior of dry-joint masonry constructions using the discrete element method (DEM). In DEM, the stone skeleton is represented via a system of individual blocks (rigid and/or deformable), interacting along their boundaries. DEM-based models have been further utilized to analyze dry-joint arches, vaults, and pier-arch systems, as discussed in [16–21].

However, most of these studies perform deterministic analysis, in which averaged material properties are used and variation in the mechanical properties of the material is neglected. Indeed, masonry is a highly heterogeneous composite material, where the material properties vary considerably within the discontinuous medium. Recent studies clearly revealed the influence of spatial and non-spatial variations of the unit and joint properties on the macro response of URM structures in terms of fracture mechanism and force-displacement behavior, as demonstrated in [22–24]. Therefore, a stochastic approach is needed to consider and quantify the variability in the material properties when analyzing URM constructions.

In this context, the present study proposes a novel stochastic discontinuum-based modeling strategy to assess the mechanical behavior, performance, and safety level of DJ-SMWs, including the uncertainties in the material properties. Furthermore, a coupled fracture energy-based contact constitutive model is implemented to improve the capabilities of the employed modeling strategy,

discussed in the following sections. Thus, the objectives of this research are summarized as follows:

- To propose a stochastic discontinuum model, simulating all possible failure mechanisms in DJ-SMWs considering the uncertainties in the material properties.
- To better understand and quantify the effect of the vertical stress level on the dry-joint walls' behavior.
- To quantify the role of interfacial frictional resistance at the joints in DJ-SMWs.
- To explore the influence of the spatial and non-spatial distribution of the contact properties in discrete element models regarding the structural behavior and force-displacement curves.
- To identify the ultimate performance limits of the DJ-SMWs and explore corresponding structural safety levels.

This paper is structured as follows. In Section 2, the computational background of DEM and the proposed contact constitutive models are presented. Then, the dry stone masonry walls, tested by Lourenço et al. [6], are analyzed for comparison purposes in Section 3. After the model validation, Section 4 presents stochastic discontinuum analyses for five vertical load levels (ranging from low to high), in which the most influential parameters affecting the failure modes and the variability in the displacement and shear force capacities are highlighted. In Section 5, a study investigating the influence of the spatial distribution of the material properties is performed, and the findings are compared to non-spatial analyses. Finally, the preliminary assessment of the performance level for the examined DJ-SMWs is discussed in Section 6, and conclusions are given in Section 7.

2 Computational Background of DEM

The structural stability of dry-joint stone masonry structures mainly relies on their self-weight, construction technique (i.e., wall cross-section morphology), and frictional resistance at the joints since no binding material or reinforcement element is used during the construction. Therefore, a detailed nonlinear structural analysis of DJ-SMWs requires the individual representation of stone

units to address the inter-block interactions. In DEM, the discrete nature of DJ-SMWs can be explicitly represented by a structured discontinuum, where each block can interact with its surrounding through contact points. However, it should be noted that within DEM formulation, any polygonal or polyhedral bodies can be utilized, which may represent the irregular geometrical configuration of the masonry construction in the structural or any constituent material level, as discussed in previous studies [25–29]. Additionally, DEM offers several distinctive features compared to FEM-based continuous and discontinuous approaches, such as automatic contact detection (*i.e.*, recognizing new contact points during the analysis) and simulating the complete detachment of blocks, prescribed as rigid or deformable. Also, rigid and deformable blocks can be used in the same model to replicate different materials and parts of the structure, which increases the computational efficiency and decrease the number of required input parameters [30,31]. The readers are referred to recent studies for further details about the differences between DEM and FEM-based applications [32,33].

Through this research, a commercial software called 3DEC developed by ITASCA [34] is used, and the user-defined contact constitutive model option is utilized to implement a recently developed contact stress-displacement law.

2.1 An overview of the numerical procedure of DEM

DEM was originally proposed to simulate the progressive failure mechanism of jointed rock masses by Cundall [35]. DEM was then employed to explore the structural behavior and capacity of various masonry structures since the early 1990s (some examples, among many others, can be found in the references [36–44]). The numerical procedure of DEM relies on the explicit time integration scheme of the governing equations of motion for the gridpoints if deformable blocks are utilized. The deformability in discrete blocks is introduced by discretizing them into finite-difference tetrahedral elements. An illustration of two deformable blocks with a defined contact point is presented in Figure 1. The motion of a deformable block can be determined via the movements of the gridpoints by integrating the equations of motion to obtain gridpoint (or node) velocities, as written in a compact form in Equation 1.

$$\dot{u}_i^{t+\Delta t/2} = \dot{u}_i^{t-\Delta t/2} + \frac{\Delta t}{m_n}\left[\Sigma F_i^t - \gamma|\Sigma F_i^t|sgn\left(\dot{u}_i^{t-\Delta t/2}\right)\right] \quad (1)$$

Here $\dot{u}_i$, m_n, γ and ΣF_i are the nodal velocity vector, lumped nodal mass, non-dimensional damping constant (by default 0.8), and summation of the force vectors, including external loads, contact forces (only for gridpoints along the block boundary), and internal nodal forces. Note that quasi-static solutions are obtained from Equation 1, considering the local damping formulation, where damping force on a node is applied proportional to the unbalanced force (ΣF_i) with a sign opposite to the motion [45].

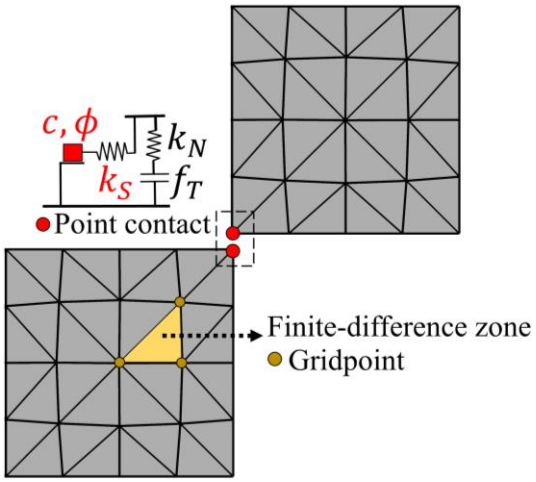

Figure 1. Illustration of the deformable blocks and point contact (in 2D).

The computed nodal velocities are used to find the new block positions and the corresponding relative point contact displacements in the tangential (u_s) and normal (u_n) directions tracked between the adjacent blocks. Then, the contact forces are obtained based on the defined contact stress-displacement law, where the calculated contact stresses are converted to forces by multiplying them with the assigned contact area. The standard contact stress update routine is summarized in Table 1, executed at each time step (Δt). The small displacement theory is utilized

in this research; therefore, only the initially recognized contact points are used in the computation cycles.

Table 1. The contact stress update routine

(**1**) The elastic contact stress increments ($\Delta\sigma$, $\Delta\tau$) are obtained via defined normal (k_N) and shear (k_S) contact stiffnesses.

$$\Delta\sigma = k_N\,\Delta u_n\,, \Delta\tau = k_S\,\Delta u_s$$

(**2**) Stress increments are added to the previous stresses (σ^0, τ^0) to compute new trial stresses (σ^n, τ^n).

$$\sigma^n = \sigma^0 + \Delta\sigma\,, \tau^n = \tau^0 + \Delta\tau$$

(**3**) σ^n and τ^n are corrected to comply with the determined failure criteria. (c and θ are the cohesion and friction angle)

$$\sigma^n < f_T\ (tensile\ strength)$$
$$|\tau^n| < c + \sigma^n\ tan\theta\ (shear\ strength)$$

Thus, a dynamic calculation scheme is performed in the pseudo time domain. At each time step, equations of motion are solved for new velocities and displacements considering the gridpoints. Then, contact forces are obtained from the relative contact deformations and corrected (if applicable) according to the failure criteria, which are then employed in the motion equations in the next time step. It needs to be highlighted that throughout this research, each stone masonry unit is represented by two adjacent deformable perfectly elastic blocks with a potential crack surface at the middle, as shown in Figure 2. A previous study of the authors addresses the sensitivity of the computational models to the number of contact points and discretization [46].

Pre-print version: Pulatsu, B., Gonen, S., Erdogmus, E., Lourenço, P.B., Lemos, J.V., and Prakash R., "*In-Plane Structural Performance of Dry-Joint Stone Masonry Walls A Spatial and Non-Spatial Stochastic Discontinuum Analysis*.", Engineering Structures (2021). **DOI**: 10.1016/j.engstruct.2021.112620

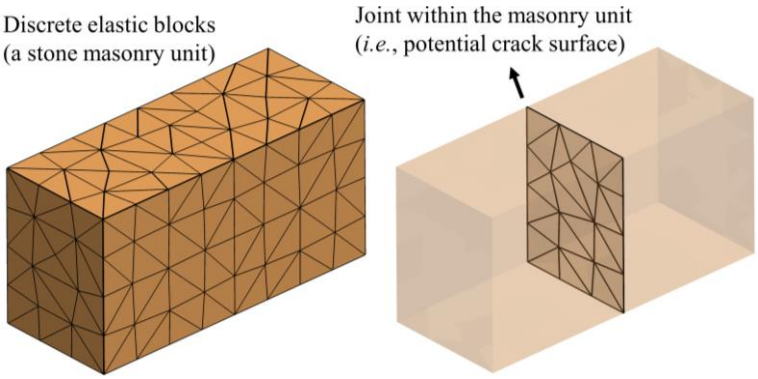

Figure 2. Representation of a typical masonry unit used in the discontinuum analysis.

2.2 Coupled (tension-shear) contact constitutive law

In the proposed discontinuum-based modeling framework, the nonlinear behavior of the blocky system is controlled by contact stress-displacement behaviors. The contact models, defined at the joints, should reflect the pre- and post-peak responses of the material under pure tension and shear, as well as combined loading scenarios. Note that two types of inter-block interaction occur mechanically at the joints: ***i***) interaction within the masonry units, ***ii***) interaction among the units. Since no binding material exists in DJ-SMWs, zero tensile strength is set to the joints among the masonry units, whereas bilinear elastic-softening behavior is implemented to be utilized within the units to allow for cracking and sliding (see Figure 3), similar to [47]. In the shear direction, the Coulomb-Slip joint model is utilized in all joints, which requires cohesion (c_0: max. (or initial) cohesion, c_{res}: residual cohesion) and friction angle (θ_0: max. (or initial) friction angle, θ_{res}: residual friction angle) parameters, shown in Figure 3. Furthermore, compression failure is not considered at the joints as it does not govern the failure mechanism under low pre-compression stress levels.

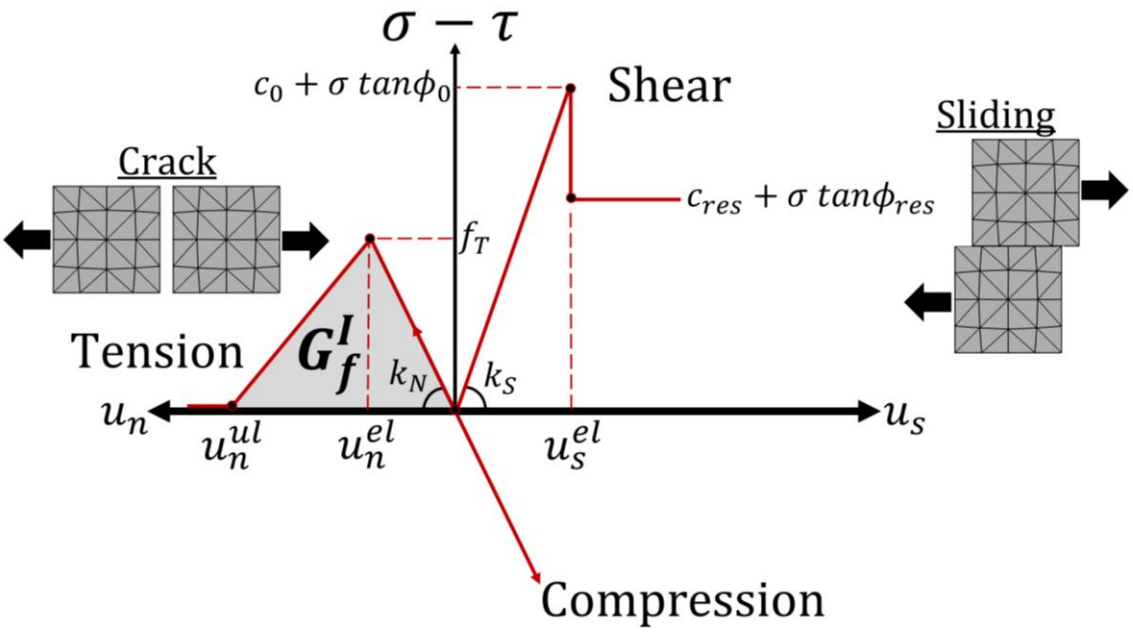

Figure 3. Contact constitutive law for stone masonry units.

The readily available cohesive contact models in 3DEC do not address the tension-shear coupling (TSC) phenomenon; hence, working as two independent (uncoupled) springs in the orthogonal directions. On the other hand, plastic damage in the tension regime should influence the shear strength if the contact deforms progressively from opening to sliding due to external forces (or vice versa). Hence, for precise simulation of this phenomenon, a coupled tension-shear contact constitutive law is implemented considering a single global damage parameter (D), following a similar analogy discussed in [48]. As given in the pseudo-code flow (Table 2), individual damage parameters for tension (d_t) and shear (d_s) are used to compute the global damage (D) developing at the contact, which helps to compute new tensile and shear strengths. Therefore, the initial failure envelope shrinks proportionally to a residual envelope considering the overall damage, influenced by contact opening and sliding failures simultaneously, demonstrated in Figure 4. The adopted contact model is written in C++ and compiled as a dynamic link library (DLL) into 3DEC software using the user-defined constitutive model option.

Pre-print version: Pulatsu, B., Gonen, S., Erdogmus, E., Lourenço, P.B., Lemos, J.V., and Prakash R., "*In-Plane Structural Performance of Dry-Joint Stone Masonry Walls A Spatial and Non-Spatial Stochastic Discontinuum Analysis*.", Engineering Structures (2021). **DOI**: 10.1016/j.engstruct.2021.112620

Table 2. Contact strength update routine implemented to couple tension and shear failures.

(1) $t^* = t_n$

(2) Compute the relative point contact displacements (both in the normal (u_n) and shear (u_s) directions)

(3) Check the tension and shear damage parameters, denoted as d_t and d_s, respectively.

$$\boldsymbol{if}\ (u_n > u_n^{el})\ \boldsymbol{then}, d_t = \frac{u_n - u_n^{el}}{u_n^{ul} - u_n^{el}};\ u_n^{el} = \frac{f_T}{u_n}\ , u_n^{ul} = \frac{2G_f^I}{f_T}$$

$$\boldsymbol{else}, d_n = 0, \boldsymbol{end_if}$$

$$\boldsymbol{if}\ (u_s > u_s^{el})\ \boldsymbol{then}, d_s = 1 \text{ (brittle failure)}$$
$$\boldsymbol{else}, d_s = 0, \boldsymbol{end_if}$$

(4) Compute coupled damage parameter

$$D = d_t + d_s - d_t d_s$$

(5) Update the contact stresses

$$f_{t,new} = f_T(1 - D)$$

$$c_{new} = c_{res} + (c_0 - c_{res})(1 - D);\ \ \theta_{new} = \theta_{res} + (\theta_0 - \theta_{res})(1 - D)$$

$$\tau_{\max,new} = \ c_{new} + \sigma^n\ tan\theta_{new}$$

(6) $t_n = t^* + \Delta t \mapsto$ go to step (1)

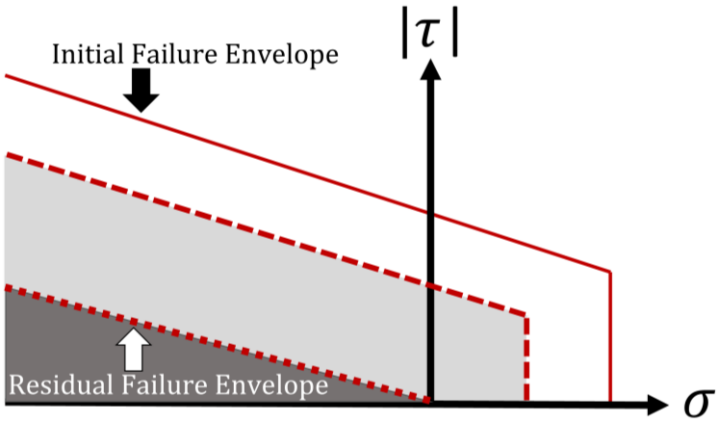

Figure 4. Initial and residual failure envelopes implemented for joints within the masonry units.

It is worth noting that a brittle failure mechanism is assumed in shear for the masonry units, which is appropriate when the units are under low pre-compression toward their longitudinal direction and compatible with the experimental observations. In the next section, validation of the

proposed modeling approach along with the difference between the coupled and uncoupled contact models are demonstrated.

3 Validation Study (Deterministic Discontinuum Analysis, D-DA)

Stone is one of the oldest natural materials (e.g., granites, sandstones, schist, and limestone), mainly used in historical constructions. However, limited experimental research is available in literature regarding the structural behavior of DJ-SMWs. In this part, dry stone masonry walls, tested by Lourenço et al. [6], are utilized for validation purposes. The experimental program was done in collaboration between the Technical University of Catalonia and the University of Minho [49]. The benchmark study comprises seven DJ-SMWs, made up of sandstone blocks (so called "Montjuic stone", a widely used local type of stone in Catalonia), subjected to combined vertical and horizontal loads. The DJ-SMWs were initially subjected to pre-compression stress, ranging from 0.15 to 1.25 MPa, and then the horizontal load was applied monotonically until reaching failure of the walls. The loading scheme and the geometrical properties of the test setup, together with the generated discrete element model, are given in Figure 5. As depicted from Figure 5, the bottom left corner of the DJ-SMWs was restrained to prevent any premature sliding failure during testing, and the reinforced concrete beam on top was let free to rotate during the horizontal loading. In the computational model, the lateral gridpoint displacements at the left toe and bottom surface are adopted as zero, and there is no restraint imposed at the top – same as the experiment, to represent the boundary conditions. The vertical loads simulated include the self-weight of the wall and the applied vertical load on the reinforced concrete beam. Furthermore, horizontal loads are exerted by imposing constant gridpoint velocities at the top surface of the loading beam (see Figure 5), where the reaction forces are extracted from these gridpoints via the implemented subroutine in the software based on FISH functions (an executable programming language in 3DEC). For further details about the testing protocol, readers are referred to [4,6,49].

Pre-print version: Pulatsu, B., Gonen, S., Erdogmus, E., Lourenço, P.B., Lemos, J.V., and Prakash R., "*In-Plane Structural Performance of Dry-Joint Stone Masonry Walls A Spatial and Non-Spatial Stochastic Discontinuum Analysis*.", Engineering Structures (2021). **DOI**: 10.1016/j.engstruct.2021.112620

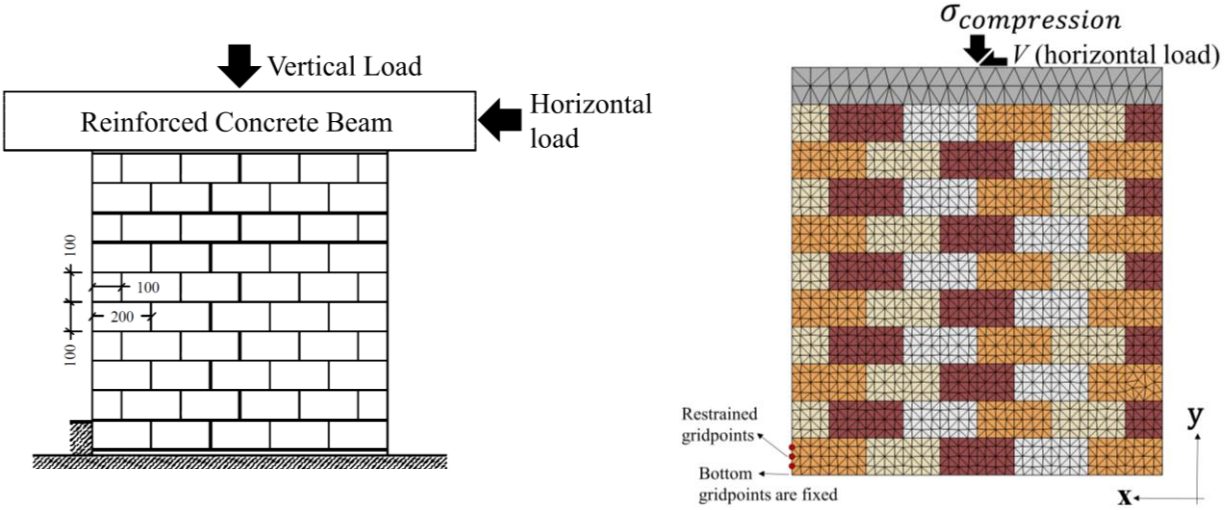

Figure 5. Illustration of the experimental setup,[6] (Left); Discrete Element Model (Right).

3.1 Force - displacement behavior: Experiment vs. D-DA

As mentioned earlier, different pre-compression loads (i.e., 30, 100, 200, and 250 kN) were considered during the testing series, which results in 0.15, 0.50, 1.00, and 1.25 MPa vertical stresses, respectively. This range of vertical stresses is chosen to represent the gravity loading in masonry structures. It should be noted that increasing the vertical pressure affected the initial stiffness of the wall (due to joint partial closure), measured for each vertical pressure prior to the lateral loading during the experiment, given in Table 3. Accordingly, in the DEM models (similar to [6]), the joint stiffness ($k_{n,j}$) is predicted by considering a series of two springs, replicating stone unit and joint, and it is calculated as written in Equation 2.

$$k_{n,j} = \frac{1}{h\left(\frac{1}{E_{DJ-SMW}} - \frac{1}{E_{stone}}\right)} \tag{2}$$

Here h, E_{DJ-SMW}, E_{stone} are the vertical spacing between horizontal joints (0.1 m), the Young's modulus of the DJ-SMW (see Table 3), and the Young's modulus of the stone unit.

Table 3. DJ-SMW initial stiffness, taken from [6].

Pre-compression stress ($\sigma_{compression}$), MPa	Wall Stiffness (E_{DJ-SMW}), MPa
0.15	566
0.50	768
1.00	1,057
1.25	1,202

The initial stiffness of the DJ-SMWs, the tensile strength of the masonry units ($f_{t,u}$), and the joint friction coefficients ($\phi_{0,j}$, $\phi_{res,j}$) are taken from the experimental results provided in [6,49]. The elastic stiffness of the stone units is determined as 15.5 GPa, and the joint dilatancy angle (ψ) is adopted as zero, as suggested in [4]. In Table 4, reference contact properties are presented, where the contact stiffness ratio between unit and joint ($\xi = k_{n,u}/k_{n,j}$) is assumed as 10, based on recommendations given in [46].

Table 4. Contact properties (discontinuum model).

Interaction **within** the masonry units (***** taken from the experiment), $v = 0.2$, $\xi = 10$				
$k_{n,u}(GPa/m)$	$k_{s,u}\ (GPa/m)$	$f_{t,u}^{*}, c_u(MPa)$	$\theta_{0,u}, \theta_{res}(°)$	$G_{f,u}^{I}\ (N/m)$*
$\xi k_{n,j}(\sigma_c)$	$k_{n,u}/2(1+v)$	3.7	35	110
Interaction **between** the masonry units ($\psi = 0°$)				
$k_{n,j}\ (GPa/m)$	$k_{s,j}\ (GPa/m)$	$f_{t,j}, c_j(Pa)$	$\phi_{0,j}\ (°)$*	$\theta_{res,j}\ (°)$*
$k_{n,j}(\sigma_c)$	$k_{n,j}/2(1+v)$	0	31.8	$\phi_{0,j}$

The reference testing series with different vertical loads clearly indicated the positive effect of the vertical load on the in-plane lateral strength of the dry joint masonry walls (Figure 6). In line with the experiments, discrete element models provide similar pre- and post-peak trends in force vs. displacement curves by accurately predicting the lateral capacity, as shown in Figure 6. Furthermore, the results of the present research are compared to other modeling approaches, namely discontinuous finite element analysis (Lourenço et al. [6]) and discrete element modeling

consisting of units with no vertical joints (Bui et al. 2017 [15]). As shown in Figure 6, the proposed representation of dry-joint walls and coupled contact constitutive laws utilized within the DEM framework lead to superior predictions, especially in the post-peak behavior.

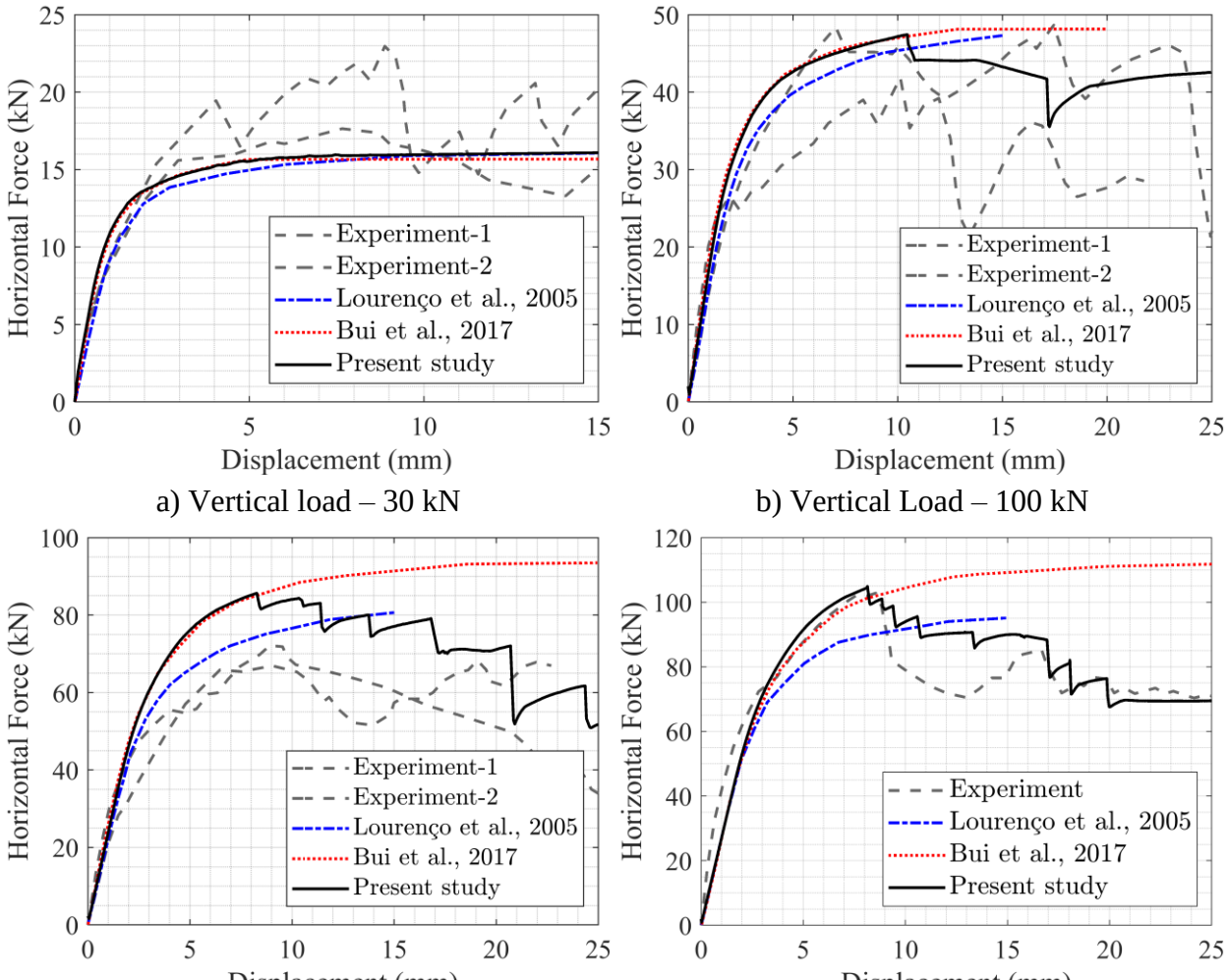

a) Vertical load – 30 kN

b) Vertical Load – 100 kN

c) Vertical Load – 200 kN

d) Vertical Load – 250 kN

Figure 6. Comparison of the proposed computational models with experimental results and other numerical simulations.

In Figure 7, the effect of the implemented coupled contact model is revealed when compared with the uncoupled contact law. It should be emphasized that in terms of maximum

force capacity, there is no significant difference between the two; however, the post-peak response of the discrete element model is in better agreement with the descending branch of the experiment when the coupled contact model is utilized. This outcome can be explained by the fact that the failure types developing within the stone units progressively shift from mode-I (traction) to mode-II (shear) mechanism when the lateral deflection of the wall increases. Coupled contact models accurately predict this phenomenon at the contact level, which also yields a better approximation at the macro level. A similar analogy, used in discontinuous FEM and DEM-based methods, can be found in [50,51].

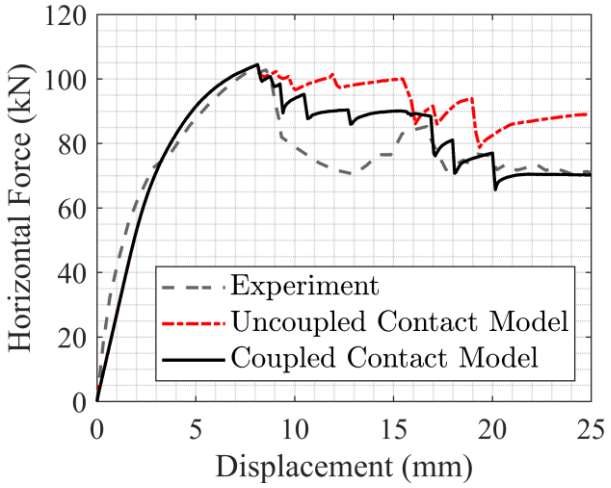

Figure 7. Effect of coupled and uncoupled tension-shear contact constitutive model on the force-displacement response of the DJ-SMW (vertical stress 1.25 MPa).

3.2 The collapse mechanism of the DJ-SMW under lateral loading

The structural behavior of tested DJ-SMWs can be grouped based on the governing failure modes, varying based on the vertical loading, as shown in Figure 8. According to the experimental observations, two distinct failure modes were dominant; *i*) ***Rocking failure***, indicating a rotational rigid body motion, which evolves as stair-step joint openings under low compression forces (e.g., 30 kN, Figure 8a), *ii*) ***Diagonal mixed-mode failure***, where there is cracking in the masonry units and noticeable joint sliding under relatively high vertical forces (vertical load $\geq$ 100 kN, Figure 8b-c). Furthermore, collapse mechanisms obtained from the discontinuum models show good agreement in terms of failure modes, which can be seen in Figure 8. However, due to the simplicity

in representing masonry units, spalling and corner failures due to high-stress concentration could not be captured, as witnessed in the higher vertical loading cases. This kind of local fracture pattern, which occurs at a much later stage of testing, can be obtained from the full discontinuous representation of the units (see [25,47,52]), instead of only one potential crack surface.

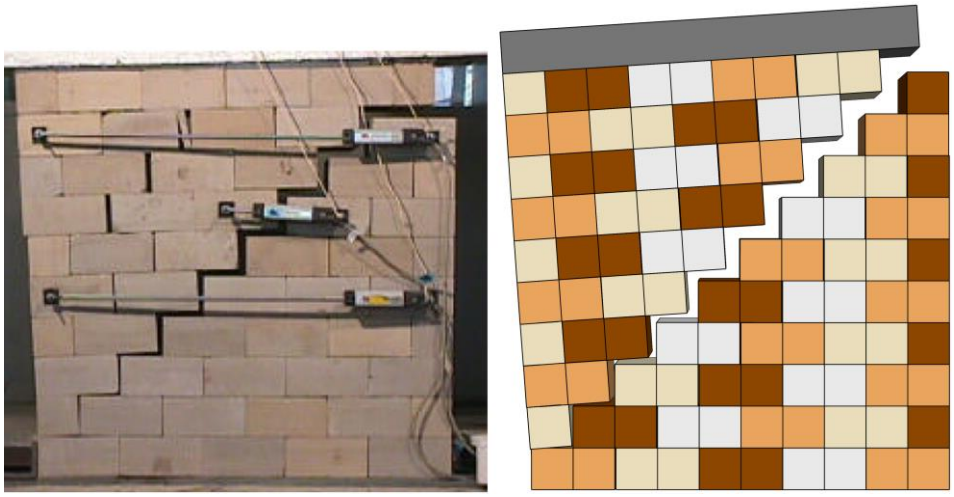

a) Experiment (Left); Discrete element model (Right) – Vertical Load 30 kN

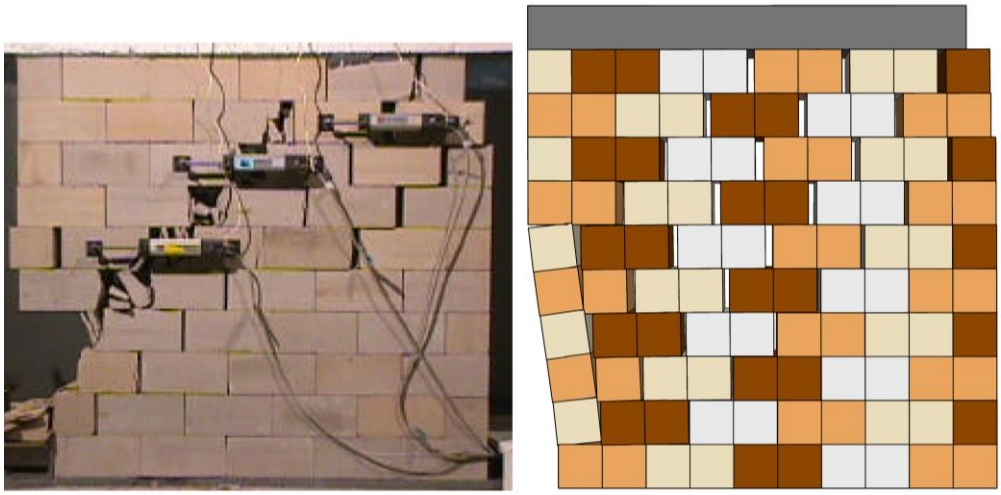

b) Experiment (Left); Discrete element model (Right) – Vertical Load 100 kN

Pre-print version: Pulatsu, B., Gonen, S., Erdogmus, E., Lourenço, P.B., Lemos, J.V., and Prakash R., "*In-Plane Structural Performance of Dry-Joint Stone Masonry Walls A Spatial and Non-Spatial Stochastic Discontinuum Analysis*.", Engineering Structures (2021). **DOI**: 10.1016/j.engstruct.2021.112620

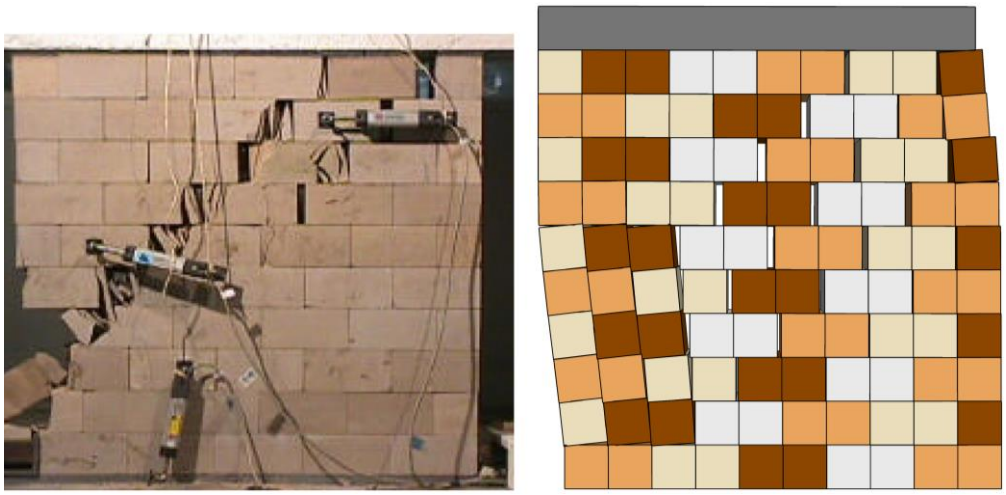

c) Experiment (Left); Discrete element model (Right) – Vertical Load 200 kN

Figure 8. Collapse mechanism of DJ-SMWs, experiment [49] vs. numerical predictions.

4 Stochastic Discontinuum Analysis (S-DA)

Masonry structures are often analyzed using deterministic methods. These methods calculate the capacity of masonry structures by considering the parameters as deterministic values despite some of those parameters being probabilistic in nature. In addition to the inherent variability of the in-situ material properties, the very same masonry specimen may yield different results depending on the test method used [53]. The stochastic approach aims to predict the possible behavior modes and evaluate how they are affected by the random model parameters. Therefore, consideration of the uncertainties in the material properties is an important step towards the probabilistic performance-based assessment of masonry structures. As an example, probabilistic seismic assessment of masonry structures, including the uncertainty in the material properties, has recently been explored by a few researchers [54–58]. However, there is still a substantial need for research to quantify the uncertainties in the analysis, both at component and system levels. For this reason, the wall adopted in the previous section for validation is now considered for a stochastic discontinuum analysis.

Pre-print version: Pulatsu, B., Gonen, S., Erdogmus, E., Lourenço, P.B., Lemos, J.V., and Prakash R., "*In-Plane Structural Performance of Dry-Joint Stone Masonry Walls A Spatial and Non-Spatial Stochastic Discontinuum Analysis*.", Engineering Structures (2021). **DOI**: 10.1016/j.engstruct.2021.112620

4.1 Uncertainty in the material and contact properties in DEM and Monte Carlo simulation

The random variables associated with the unit and joint properties are considered in the probabilistic analyses, including the stiffness of joints ($k_{n,j}$), the stiffness of units ($k_{n,u}$), the tensile strength of units ($f_{t,u}$), the friction angle within units ($\phi_{0,u}$), and the friction angle for joints ($\phi_{0,j}$). The cohesion of the units (c) is implicitly taken as a random variable, as it is set equal to the tensile strength of units (see Table 4). The random variables, the assigned statistical distributions, and their distribution parameters are presented in Table 5. Note that the stiffness values presented in this table are the multipliers for stiffness, whereas the mean values of other parameters are taken from Table 4. Normal distribution was assumed for the elastic stiffness and friction angle parameters, following the pertinent literature [22,57,59,60]. The tensile strength of the masonry units is assigned with a lognormal distribution to prevent negative values during sampling, with a slightly higher coefficient of variation given the larger scatter found in tests.

Table 5 Random variables and the assigned distributions

Random Variable	Probability Distribution	Mean (μ)	Coefficient of Variation	Lognormal mean (μ_{ln})	Lognormal Std. Dev. (σ_{ln})
$k_{n,j}$ (contact stiffness defined for the joints)	Normal	1	0.25	N/A	N/A
$k_{n,u}$ (contact stiffness defined for the units)	Normal	1	0.25	N/A	N/A
$f_{t,u}$ (unit tensile strength)	Lognormal	3.7	0.30	1.265	0.294
$\phi_{0,u}$ (friction angle – units)	Normal	35.0	0.20	N/A	N/A
$\phi_{0,j}$ (friction angle - joints)	Normal	31.8	0.20	N/A	N/A

After the statistical distributions are determined, the Latin Hypercube Sampling (LHS) method is utilized to derive sample values for the simulations. No correlation is assumed between the parameters. Five vertical pre-compression stress scenarios are considered 0.15, 0.50, 0.75, 1.00, and 1.25 MPa. This means that one additional intermediate pre-compression load level is

considered to broaden the range of the experimental testing discussed in the previous section. Fifty samples are used for each load case, resulting in 250 samples for each random variable in total. The corresponding histograms and probability distributions of the input variables for all samples are presented in Figure 9. The Latin Hypercube Sampling method is a variation of Monte Carlo Simulation (MCS) and a stratified variance reduction technique. By segmenting the variable's probability distribution into a number of equal-probability and non-overlapping intervals, the MCS sample variance is reduced, and the number of required simulations is lowered [61]. The samples obtained by the LHS fill the sample space more effectively due to being taken within those intervals. This decreases the variance of statistical estimators computed from the samples [62]. The LHS technique has been used as a tool to improve the efficiency of sampling methods for structural reliability analysis and has been shown to produce significant savings on computational cost [63].

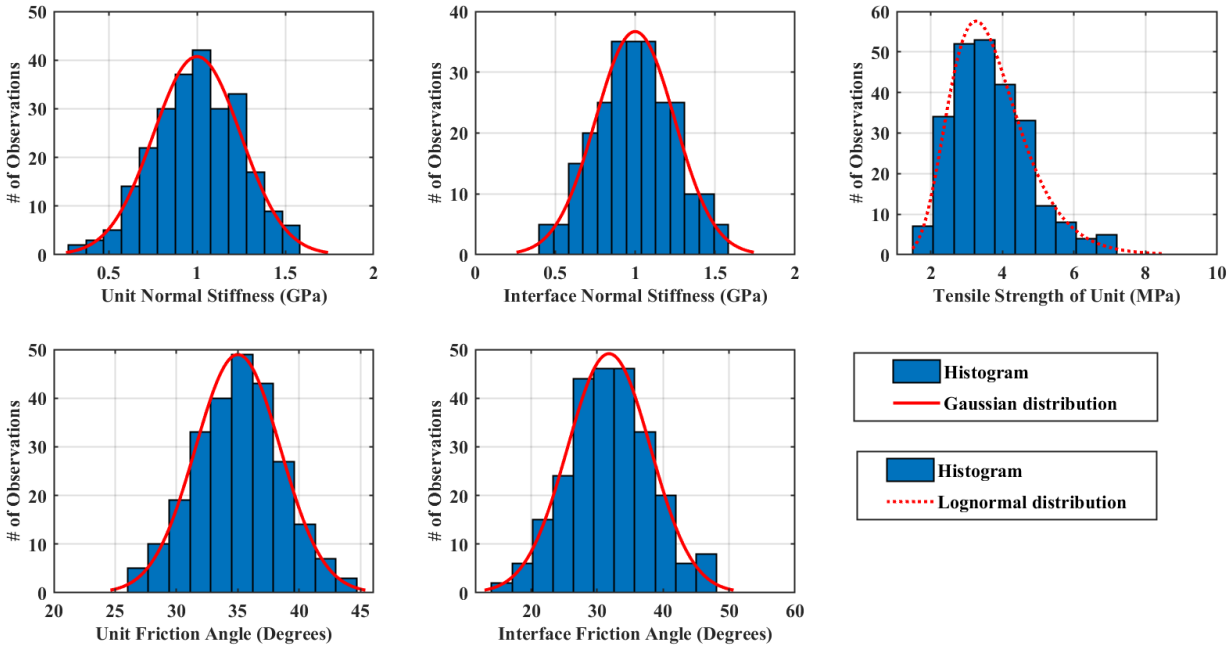

Figure 9. Histograms and probability distributions of the sampled random variables

A total of 250 simulations are conducted to obtain random parameters, and the number of simulations, 50 for each load case, is decided by observing the samples' mean and standard deviation. The relative difference between the prescribed mean values (in Table 5) and the mean

values after "*j*" simulations are tracked to define the sufficient number of simulations. This relative difference is expressed in terms of percent error, and its magnitude for the pre-compression stress level of 0.15 MPa is illustrated in Figure 10. The final values of the errors for each case are smaller than 0.2% for all random variables.

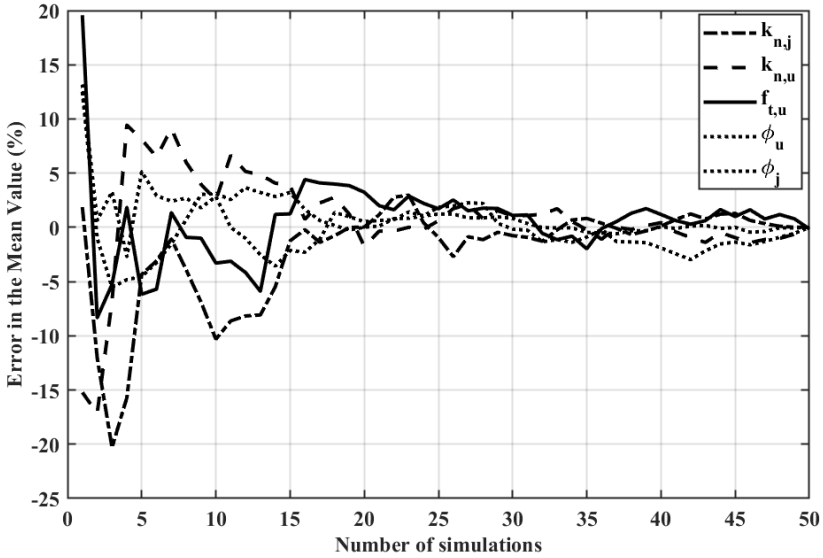

Figure 10. Example of error in the mean values after *j* number of simulations –(vertical stress of 0.15 MPa)

4.2 Stochastic discontinuum analysis (S-DA)

Stochastic analyses resulted in two distinct behavior types: rocking and mixed-mode, as mentioned earlier. The well-known flexure/rocking mechanism is characterized by overturning the wall in the applied load direction. On the other hand, the mixed-mode involves the cracking in the units and sliding in the bed-joints, commonly referred to as diagonal shear [64]. The force-displacement behavior of the dry-joint masonry walls for each case is presented in Figure 11. Each mode of failure indicates a similar force-displacement graph with a variation. For instance, the rocking mode has a smooth plateau after the inelastic behavior starts, and it sustains the load-carrying capacity until the equilibrium is lost, whereas the mixed-mode yields more complex behavior with several stress-drops due to cracking in the units, sliding at the joints, which yields a softening regime in the post-elastic behavior, as can be observed in Figure 5c. The ultimate lateral displacement is usually adopted as the point on the load-displacement curve where the ultimate load drops to 80% of the maximum load, which is not present in the rocking mechanism.

Some rare cases demonstrate a damage mechanism similar to the mixed-mode along with a force-displacement graph similar to a rocking mode. Moreover, some of the mixed-mode graphs include several drops and rises, oscillating around 80% of the maximum force. Such results are expected from the stochastic analyses and should be interpreted together with the failure mechanism obtained from the simulation.

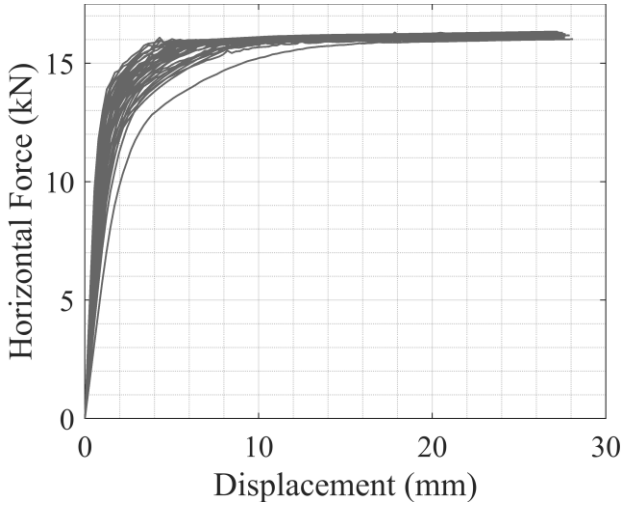

a) Rocking mechanism (vertical stress: 0.15 MPa)

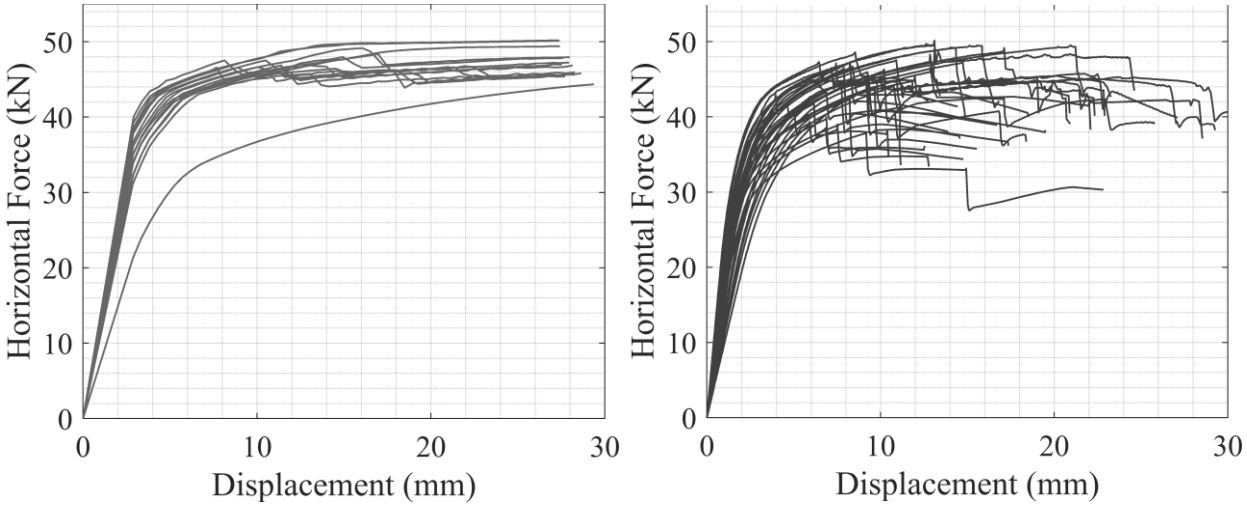

b) **Left**: Rocking; **Right**: Diagonal mixed-mode failure mechanisms (vertical stress 0.50 MPa)

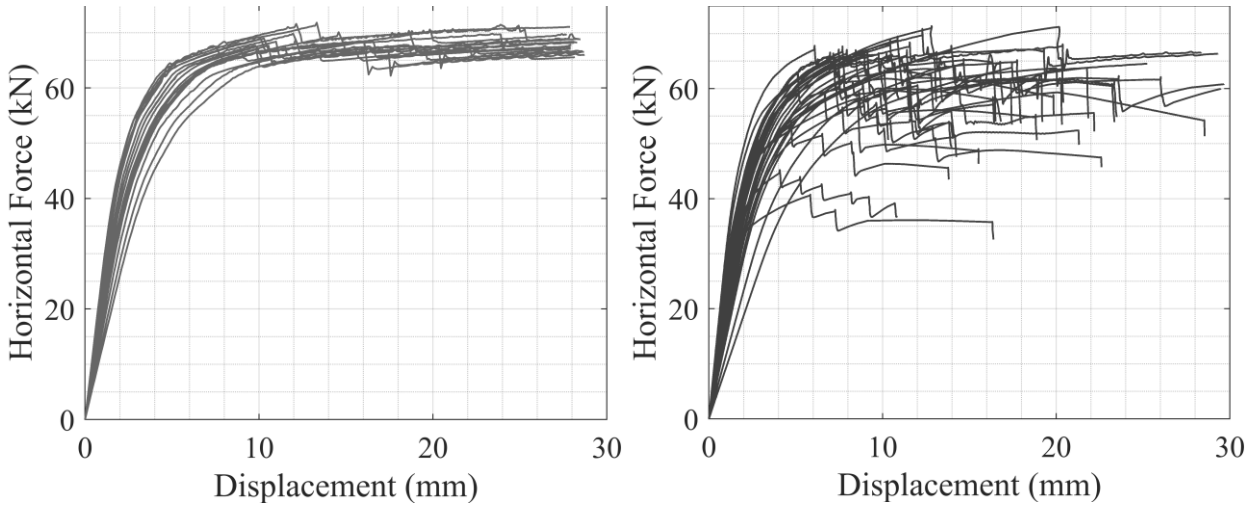

c) **Left**: Rocking; **Right**: Diagonal mixed-mode failure mechanisms (vertical stress 0.75 MPa)

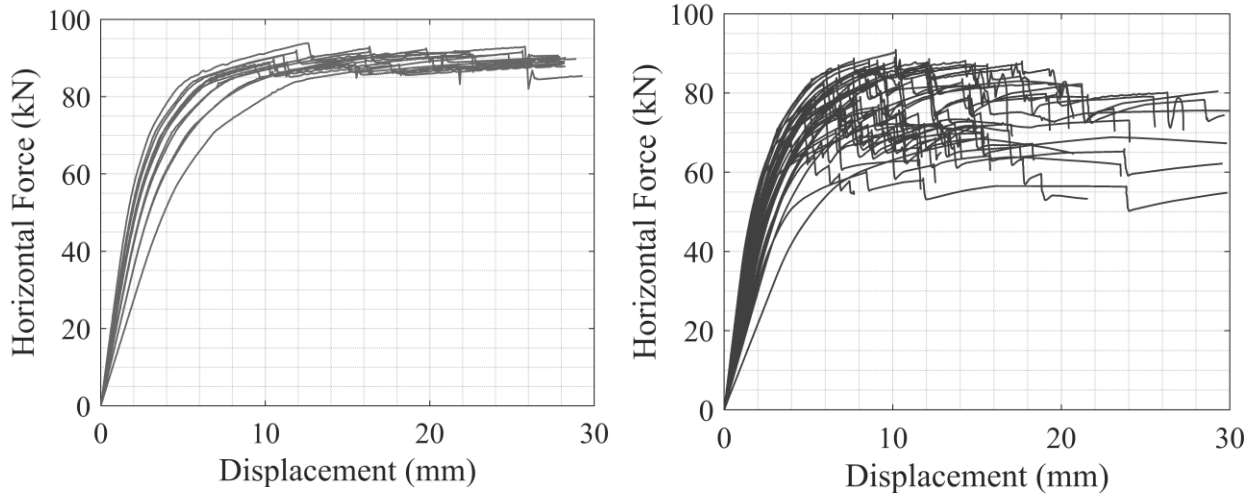

d) **Left**: Rocking; **Right**: Diagonal mixed-mode failure mechanisms (vertical stress 1.00 MPa)

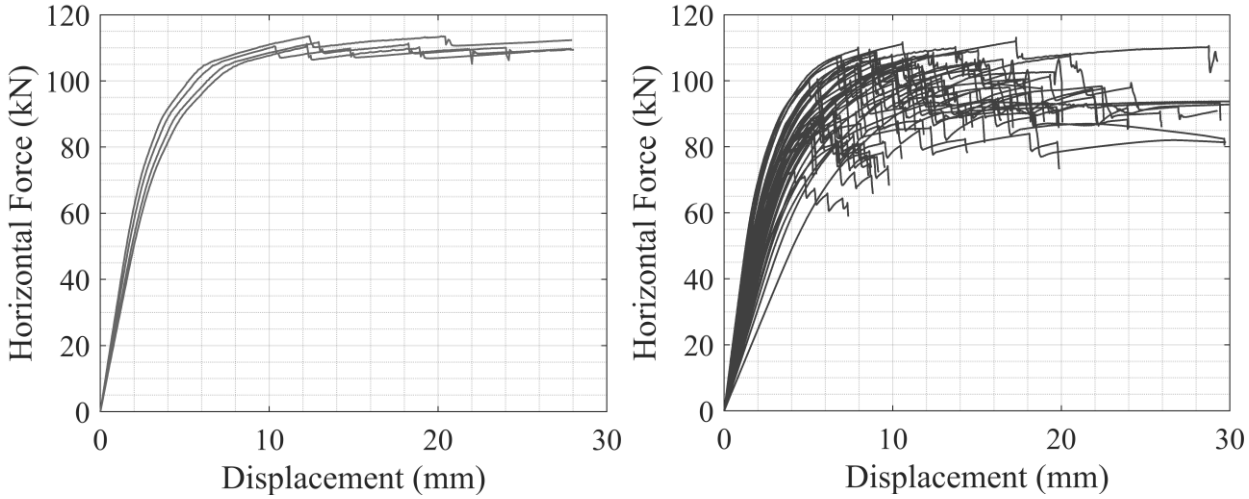

e) **Left**: Rocking; **Right**: Diagonal mixed-mode failure mechanisms (vertical stress 1.25 MPa)

Figure 11. Failure mechanisms of DJ-SMWs under combined compression-shear forces.

The results highlight the pronounced effect of the vertical stress level both in the capacity and behavior of the DJ-SMWs. With the increasing vertical stress, the maximum lateral load capacity increased significantly for both modes of failure. This well-known phenomenon can be seen in Table 6 and Table 7 and was also observed in extensive experimental work on unreinforced masonry walls [6,64,65]. On the other hand, the increasing vertical load may yield an adverse effect on the maximum displacement capacity when the failure occurs as a mixed-mode. The percentage of rocking mode occurrences decrease with increasing vertical stress. From vertical stress of 0.50 MPa to 1.25 MPa, the probabilities of rocking mode are 28%, 34%, 28%, and 8%, respectively. Thus, from a statistical point of view, it is less likely to obtain a rocking failure if the vertical stress is increased further for a given set of parameters and testing conditions.

Table 6. Average values of the input parameters for ***rocking failure*** mode and corresponding maximum average force and displacement.

	Average Values			
Vertical Stress (MPa)	ϕ_j **(*degrees*)**	$f_{t,u}$ **(*MPa*)**	$Force_{max}$ **(*kN*)**	$Disp_{max}$ **(*mm*)**
0.15	31.80	3.69	16.24	27.54
0.50	38.13	3.86	47.71	28.08
0.75	38.09	3.66	69.51	28.21
1.00	38.36	4.53	91.58	28.24
1.25	39.05	4.45	112.13	27.96

Table 7. Average values of the input parameters for ***mixed-mode failure*** and corresponding maximum average force and displacement.

	Average Values			
Vertical stress (MPa)	ϕ_j **(*degrees*)**	$f_{t,u}$ **(*MPa*)**	$Force_{max}$ **(*kN*)**	$Disp_{max}$ **(*mm*)**
0.15	Failure mode non-occurring			
0.50	29.41	3.62	45.90	18.34

0.75	28.72	3.71	63.89	19.47
1.00	29.57	3.44	80.97	17.93
1.25	31.17	3.63	100.72	16.26

4.3 Influence of the contact properties on the macro-behavior of the DJ-SMWs

In this section, the effects of essential nonlinear input parameters are explored for each vertical stress, focusing on the failure mechanism and lateral load-carrying capacity of the DJ-SMWs.

Failure mechanism: This research indicates that the frictional resistance at the joints plays a major role in the local and global failure mechanism of the DJ-SMWs. As can be seen from Table 6 and Table 7, there is a certain threshold between two distinct failure mechanisms related to the joint friction angle, especially from moderate (0.5 MPa) to high level of vertical stress (1.25 MPa). Table 6 indicates that rocking failure is associated with relatively high joint friction angles (e.g., $\phi_j \geq 38°$), whereas mixed-mode failure occurs where the average joint friction angle is lower than 32° (see Table 7). Another observation reveals that when the vertical stress level is high, the rocking mode is associated with higher unit tensile strength. In contrast, for the mixed-mode failure, there is no correlation found between the unit tensile strength and the vertical loading.

In-plane lateral capacity: The effect of the model parameters on the lateral load capacity is investigated by tracking the changes in the maximum lateral load with respect to the mean values of the model parameters. The outcome is presented in Figure 12 for the joint and unit friction angle (ϕ_j, ϕ_u) and unit tensile strength ($f_{t,u}$) as they produced specifically meaningful results.

The results indicate a strong correlation of the lateral load capacity with the joint friction angle for all pre-compression stress levels, shown in Figure 12. Furthermore, the relationship between the in-plane lateral load capacity and the unit tensile strength shows a complex relationship in mixed-mode mechanism. Figure 12 points out that unit tensile strength value may only be partly correlated with lateral load capacity when the DJ-SMWs are subjected to high vertical pressures (i.e., ≥1.00 MPa). Furthermore, there is no correlation between the unit friction angle and the lateral load capacity; however, this situation should be interpreted with caution given that, in the proposed computational approach, the masonry units have a single vertical surface for potential

cracks and sliding failures. Last but not least, there is no direct correlation observed between the displacement capacity and the examined parameters.

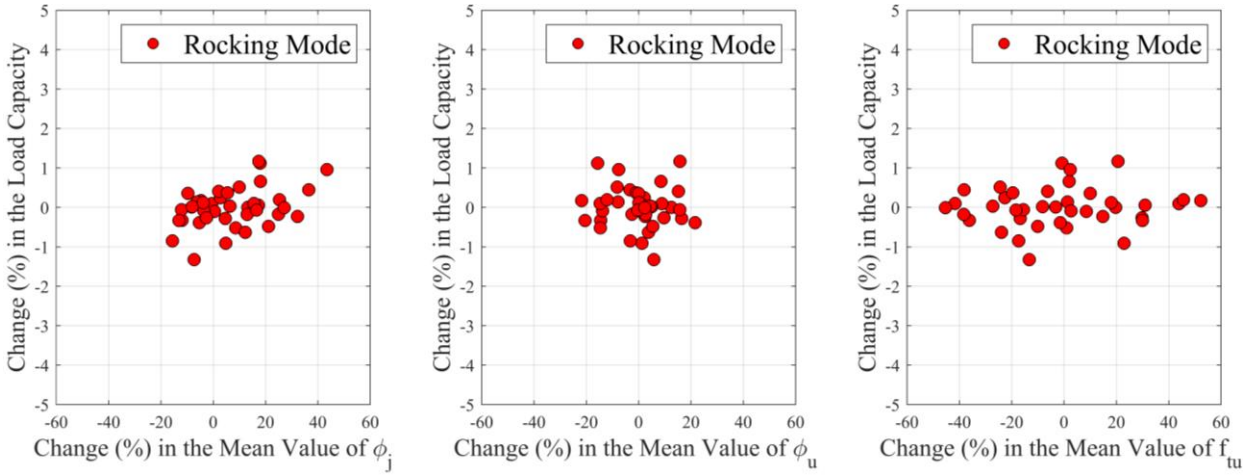

a) Vertical stress 0.15 MPa

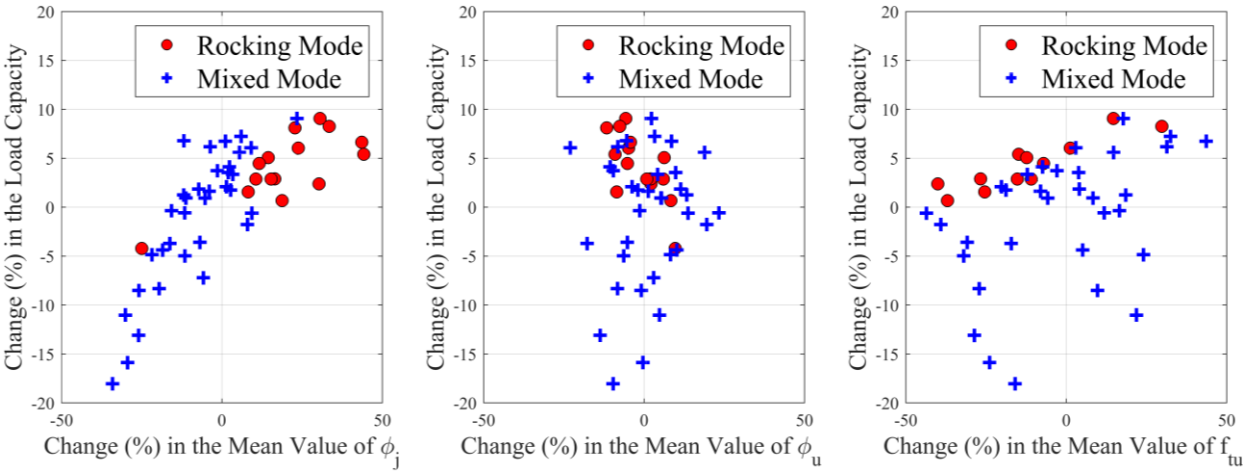

b) Vertical stress 0.50 MPa

Pre-print version: Pulatsu, B., Gonen, S., Erdogmus, E., Lourenço, P.B., Lemos, J.V., and Prakash R., "*In-Plane Structural Performance of Dry-Joint Stone Masonry Walls A Spatial and Non-Spatial Stochastic Discontinuum Analysis*.", Engineering Structures (2021). **DOI**: 10.1016/j.engstruct.2021.112620

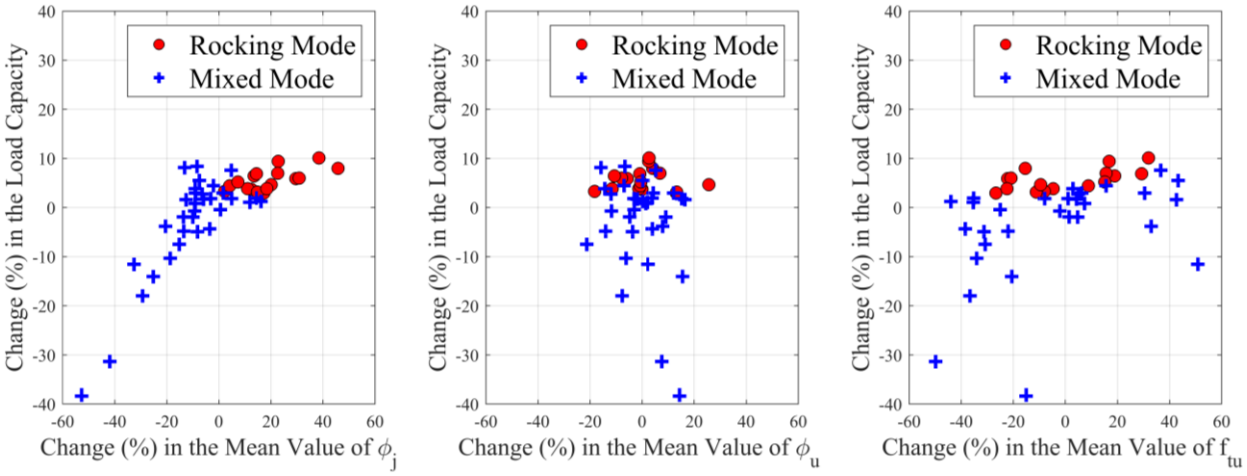

c) Vertical Stress 0.75 MPa

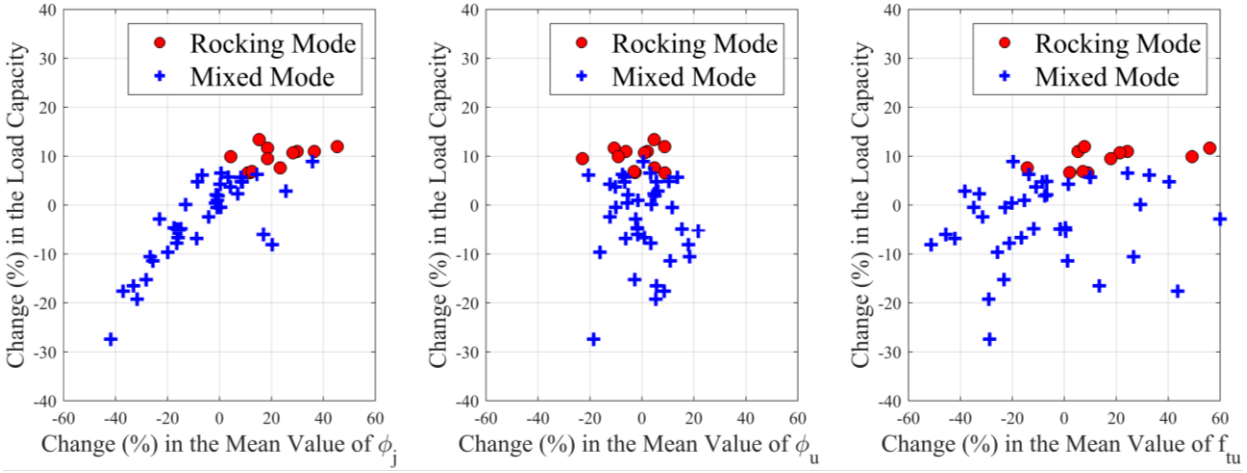

d) Vertical stress 1.00 MPa

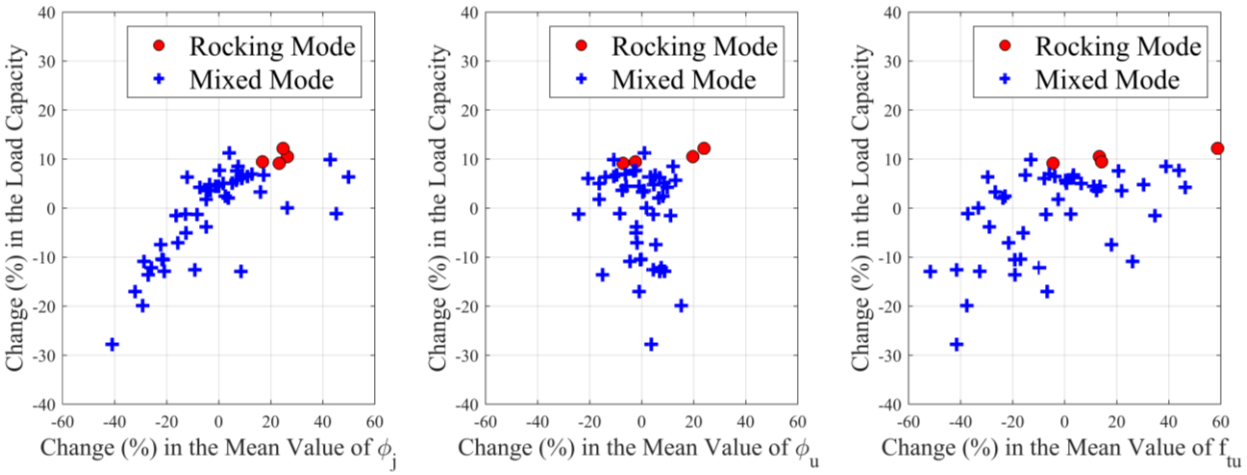

e) Vertical stress 1.25 MPa

Figure 12. Influence of the joint friction angle (ϕ_j), friction angle at the unit-joint interfaces (ϕ_u) and tensile strength of the units ($f_{t,u}$) on the capacity and failure mechanism distributions.

Pre-print version: Pulatsu, B., Gonen, S., Erdogmus, E., Lourenço, P.B., Lemos, J.V., and Prakash R., "*In-Plane Structural Performance of Dry-Joint Stone Masonry Walls A Spatial and Non-Spatial Stochastic Discontinuum Analysis*.", Engineering Structures (2021). **DOI**: 10.1016/j.engstruct.2021.112620

5 Spatial S-DA and Non-Spatial S-DA

The mechanical properties of masonry components vary spatially within the discontinuous domain of the structure. These changes stem from the inherent variability of the material properties, workmanship, and the uneven degradation of materials and joints. The degree of the spatial variability of the properties, however, is unknown. To investigate this effect, stochastic discontinuum analyses incorporating the spatial variability of the random parameters, given in Table 4, are carried out considering vertical stress of 0.75 MPa, which corresponds to a moderate level. In the analysis, each joint is given an identification number as illustrated in Figure 13a, where the joints within and in-between the units are grouped separately. Then, different tensile strengths and different frictional resistance were considered for each joint (see Figure 13b). The sampling of the parameters for the units and joints is done using the LHS method and the distributions previously assigned for each parameter (Table 5).

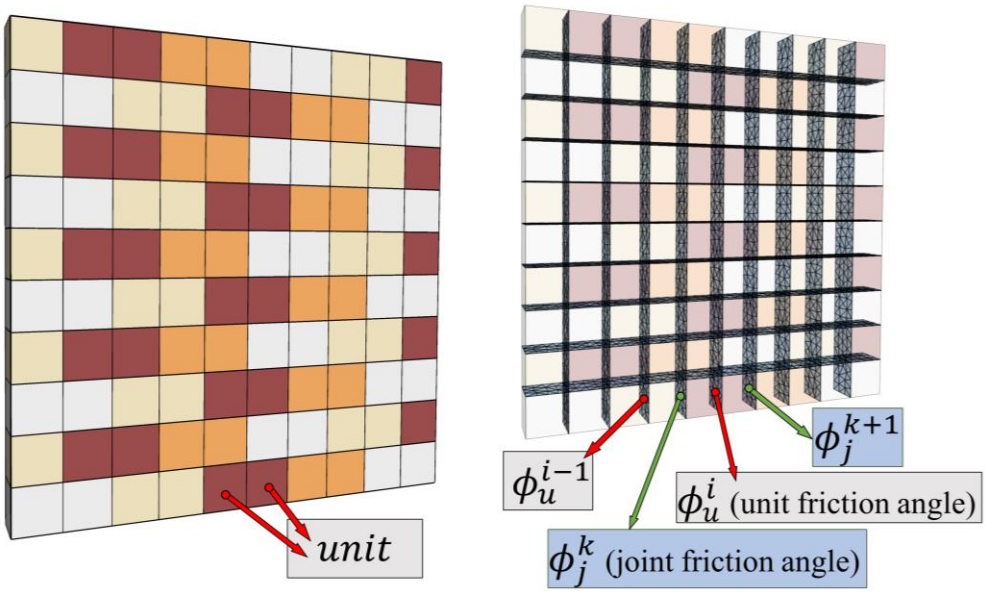

a) Contact surface numbering for unit and joints, $i \in [1..45]; k \in [1..135]$.

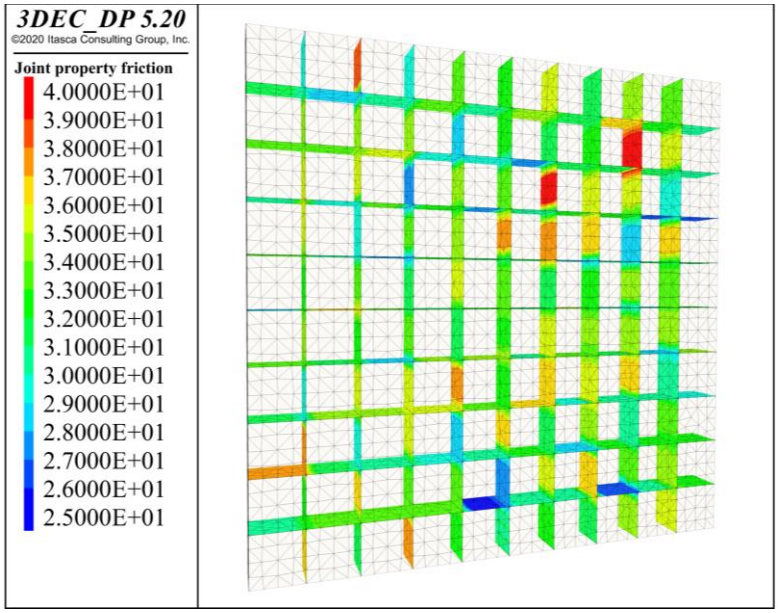

b) An example showing the spatial distribution of friction angles

Figure 13. Illustration of the contact surface numbering and spatial variation of the contact friction angle values.

Hence, in a single simulation, a number of values equal to the number of joints are sampled from the specified distribution. Through spatial S-DA, 100 discrete element models are run. The sampling process is repeated for each of the 100 simulations. Note that the number of runs for each case (i.e., 50) is doubled to account for the increased variability of the parameters within the structure. In line with the previous results, the force-displacement curves are separated for rocking and mixed failure modes, as illustrated in Figure 14.

Pre-print version: Pulatsu, B., Gonen, S., Erdogmus, E., Lourenço, P.B., Lemos, J.V., and Prakash R., "*In-Plane Structural Performance of Dry-Joint Stone Masonry Walls A Spatial and Non-Spatial Stochastic Discontinuum Analysis*.", Engineering Structures (2021). **DOI**: 10.1016/j.engstruct.2021.112620

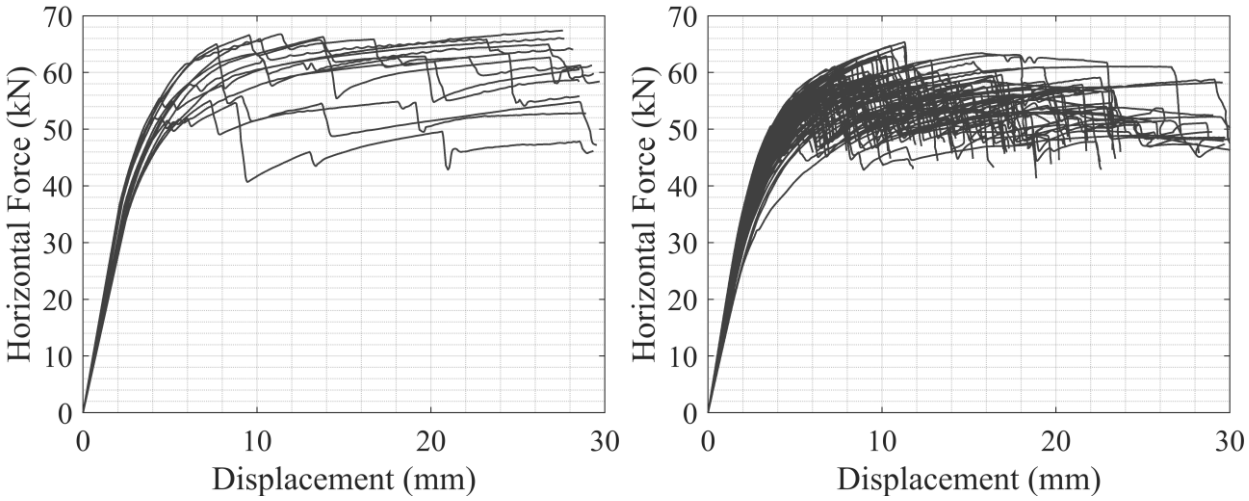

a) FM: Rocking b) FM: Diagonal Mixed Mode

Figure 14. Failure mechanism (FM) of DJ-SMWs (vertical stress: 0.75 MPa, spatial S-DA)

Comparing the average values of the maximum force and displacements, given in Table 8, to the non-spatial S-DA, it is observed that these values decreased slightly. The spatial S-DA produces more consistent results and indicates fewer rocking failures (12%) than the non-spatial analyses (34%). However, it is hard to point out which approach (the spatial or non-spatial S-DA) is more appropriate at this stage due to the limited repetitions in experimental data. Note that non-spatial S-DA is also a part of spatial analysis, representing the cases where the parameters are distributed with much less variance.

Table 8. Average maximum force and displacement obtained from spatial and non-spatial S-DA (spatial analysis is denoted as 0.75*).

Vertical stress (MPa)	**Average Values**			
	Rocking		**Mixed Mode**	
	$Force_{max}$ **(kN)**	$Disp_{max}$ **(mm)**	$Force_{max}$ **(kN)**	$Disp_{max}$ **(mm)**
0.15	16.24	27.54	N/A	
0.50	47.71	28.08	45.90	18.34
0.75	69.51	28.21	63.89	19.47
0.75*	63.17	28.80	57.29	17.00
1.00	91.58	28.24	80.97	17.93
1.25	112.13	27.96	100.72	16.26

Pre-print version: Pulatsu, B., Gonen, S., Erdogmus, E., Lourenço, P.B., Lemos, J.V., and Prakash R., "*In-Plane Structural Performance of Dry-Joint Stone Masonry Walls A Spatial and Non-Spatial Stochastic Discontinuum Analysis*.", Engineering Structures (2021). **DOI**: 10.1016/j.engstruct.2021.112620

6 Towards Performance Assessment of Dry-Joint Stone Masonry Walls

There are no standardized or widely accepted criteria for performance assessment of dry-joint masonry walls. In the Turkish Building Seismic Code (TBDY 2018) [66], no criteria are available for the DJ-SMWs, and the performance assessment of unreinforced masonry buildings is solely based on the percentage of the walls failing to resist the shear forces generated during seismic actions. Similarly, stone masonry is beyond the scope of ASCE 41-17 [67]. Even though a few researchers attempted to define performance limits for historical stone masonry structures [68–70], only one of them [71] considered dry-joint stone masonry construction. Therefore, this study is a first step to the ultimate goal of setting seismic performance criteria for dry-joint stone masonry walls. In order to determine the seismic performance of structural walls, their response to the seismic actions (capacity, displacement capacity, failure mode, ductility, etc.) should be estimated. For this reason, the effects of the vertical stress level and uncertain material parameters on the collapse mechanisms and the variability of maximum lateral force and displacement based on the stochastic discontinuum analysis are discussed. The discussion is focused on the seismic behavior and the variability of the response parameters in the following paragraphs.

A ductile response of the load-bearing masonry walls is desired to obtain good seismic behavior and high energy dissipation. In this regard, the rocking behavior provides ductility, as the maximum lateral load is sustained for larger displacements. It dissipates energy through impact and maintains the walls' integrity except for the localized damage at the corners. On the other hand, the mixed-mode (diagonal shear cracking) displays a more brittle behavior, which may be associated with catastrophic failure [64], in case the displacement demand is high. For the cases investigated in this study, it is observed that the mixed-mode behavior does not always behave in a brittle fashion, as several cases of ductile force-displacement curves are noticed in Figure 11. Still, the average maximum displacement is significantly less for a mixed-mode type of failure when compared with the rocking mode. Therefore, a correct prediction of the failure mode is essential for an accurate prediction of deformation capacity.

Pre-print version: Pulatsu, B., Gonen, S., Erdogmus, E., Lourenço, P.B., Lemos, J.V., and Prakash R., "*In-Plane Structural Performance of Dry-Joint Stone Masonry Walls A Spatial and Non-Spatial Stochastic Discontinuum Analysis*.", Engineering Structures (2021). **DOI**: 10.1016/j.engstruct.2021.112620

The average force-displacement curves obtained for different vertical stresses (denoted as $\sigma_i, i \in [1..5]$, and spatial S-DA is denoted as σ_3^*) are provided in Figure 15. Both for rocking and mixed-mode failure mechanisms, the positive influence of the vertical stress level on the maximum lateral load capacity is clearly shown. The increase in the stiffness of the walls with increasing vertical stress is also noticed. This phenomenon was also reported by other researchers [71,72]. In the rocking failure (Figure 15a), the maximum displacements are similar, and the maximum force variation is small, approximately 10% for all load cases, indicating a more predictable behavior. On the other hand, in the mixed-mode failure (Figure 15b), considering the uncertainty in the material properties yields significant alteration of the seismic displacement capacity of dry-joint stone masonry walls. The coefficient of variation for the ultimate displacement ranged between 30-50% for different vertical stress levels. This large variation is one of the important deformation characteristics of masonry walls and was also observed in experimental studies [71,73]. Thus, if the performance levels are defined in terms of drifts, the large scatter in the results is expected to pose problems.

Finally, the results indicate a good correlation with the experimental findings on DJ-SMWs in the literature. The analyzed DJ-SMWs under monotonic loading maintain their lateral load capacity (80% of the maximum force is set as a limit) until the drift ratios of at least 2.5% and 1.5% for rocking and mixed modes failure, respectively (see Figure 15). The ultimate drift values for the same type of walls under cyclic loading are proposed as 2.3% and 1.5% for rocking and mixed modes failure, respectively, in extensive experimental research campaigns on stone masonry walls [71]. Note that for the drift uncertainty, the same study proposes a similar coefficient of variation, 40% for the ultimate drift, which also justified the adoption of much lower drift limits in performance-based seismic assessment codes.

Pre-print version: Pulatsu, B., Gonen, S., Erdogmus, E., Lourenço, P.B., Lemos, J.V., and Prakash R., "*In-Plane Structural Performance of Dry-Joint Stone Masonry Walls A Spatial and Non-Spatial Stochastic Discontinuum Analysis*.", Engineering Structures (2021). **DOI**: 10.1016/j.engstruct.2021.112620

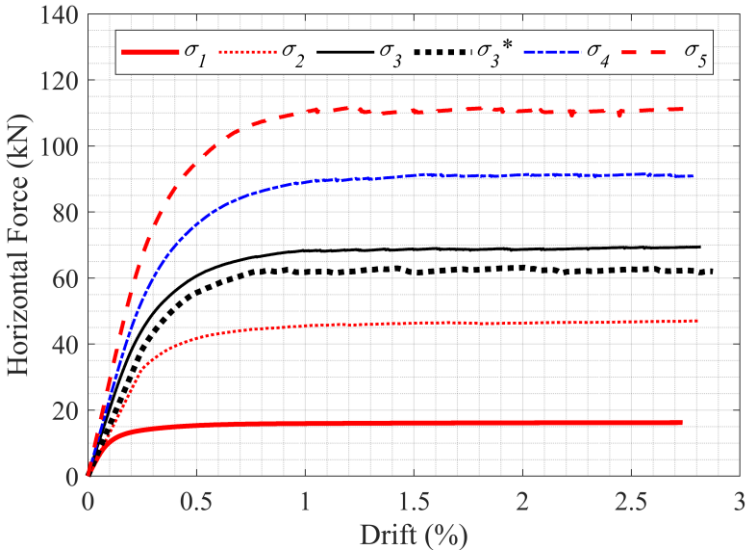

a) Rocking mechanism

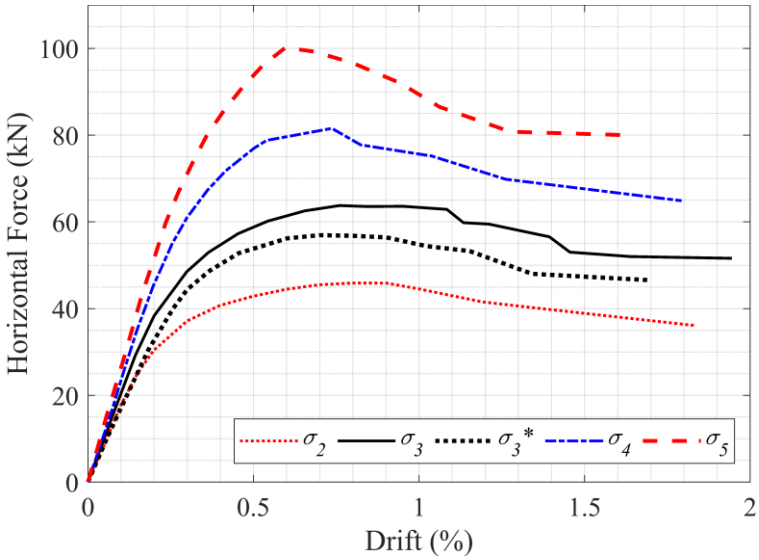

b) Mixed failure mode

Figure 15. Mean force vs. drift curves of DJ-SMWs for rocking and mixed failure modes under different vertical pre-compression conditions ($\sigma_1 = 0.15, \sigma_2 = 0.50, \sigma_3 = 0.75, \sigma_3^* = 0.75\ (spatial\ S-DA), \sigma_4 = 1.00, \sigma_5 = 1.25\ MPa$)

7 Conclusions

The dry-joint stone masonry constructions constitute an important part of existing built cultural heritage, demonstrated to be rather vulnerable to seismic actions. This research presents a spatial and non-spatial stochastic discontinuum analysis strategy based on the discrete element

method to assess DJ-SMWs under in-plane (monotonic) lateral loading. The stochastic approach adopted in this research systematically scans the random parameters to which the response is sensitive. It also aims to determine the performance limits of dry joint masonry walls under given conditions. Therefore, the proposed methodology is novel to the literature even though stochastic micro-modeling or DEM analyses have been conducted for other types of structures. Based on the findings, the following conclusions are drawn.

- The proposed coupled fracture energy based contact constitutive law proposed to model discrete interfaces better captures the post-peak behavior of the DJ-SMWs. Furthermore, the predicted failure mechanisms and force-displacements curves are in good agreement with previously published experimental and analytical results.
- The obtained results from S-DA can be grouped in two failure modes, i.e., rocking and mixed-mode (diagonal shear), where the frequency of the rocking mechanism significantly decreases when the vertical pressure over the DJ-SMWs increases.
- It is demonstrated that the joint friction angle and the vertical stress have a pronounced influence on the failure mechanism and capacity of the DJ-SMWs, whereas unit tensile strength and the lateral capacity can only be correlated in the case of high vertical loads, in which cracking of the stone units becomes more relevant for the response.
- Spatial S-DA provides less variant force-displacement curves than non-spatial S-DA and represents the heterogeneous characteristics of masonry by explicitly considering different mechanical properties at the joints and unit-joint interfaces.
- The preliminary performance assessment indicates that analyzed DJ-SMWs can maintain lateral loads up to 2.5% and 1.5% drifts on average for rocking and mixed-mode failure mechanisms, respectively, when considering the given workmanship, boundary conditions, and material properties. The coefficient of variation of the drift is quite large (between 30 and 50% according to the vertical stress level), meaning that safer limits are needed in standards, or alternative parameters need to be considered.

Finally, the proposed modeling approach validated using the experimental results can simulate the discontinuous displacement field within the DJ-SMW domain by revealing local and global damage mechanisms. Therefore, it can further investigate the effects of various setups and

structural configurations, which yields a great economy in performing such a comprehensive study computationally instead of a very broad and costly experimental campaign.

Different boundary conditions, aspect ratio, and morphology of the stone masonry walls need to be considered in future studies. Furthermore, cyclic shear and dynamic tests are of relevance to consider the rate-dependent behavior of DJ-SMWs. Finally, to eliminate the pre-defined cracking surface in units, which is a limitation of the proposed computational model, masonry units may be replicated via randomly generated polyhedral blocks, allowing irregular crack propagation in units (*e.g.*, diagonal cracks and unit-corner failures).

8 References

[1] Costamagna E, Santana Quintero M, Bianchini N, Mendes N, Lourenço PB, Su S, et al. Advanced non-destructive techniques for the diagnosis of historic buildings: The Loka-Hteik-Pan temple in Bagan. J Cult Herit 2020;43:108–17. doi:10.1016/j.culher.2019.09.006.

[2] Vlachakis G, Vlachaki E, Lourenço PB. Learning from failure: Damage and failure of masonry structures, after the 2017 Lesvos earthquake (Greece). Eng Fail Anal 2020;117:104803. doi:10.1016/j.engfailanal.2020.104803.

[3] Akkar S, Aldemir A, Askan A, Bakir S, Canbay E, Demirel IO, et al. 8 March 2010 elaziğ-kovancilar (Turkey) Earthquake: Observations on ground motions and building damage. Seismol Res Lett 2011;82:42–58. doi:10.1785/gssrl.82.1.42.

[4] Lourenço PB, Ramos LF. Characterization of Cyclic Behavior of Dry Masonry Joints. J Struct Eng 2004;130:779–86. doi:10.1061/(asce)0733-9445(2004)130:5(779).

[5] Vasconcelos G, Lourenço PB. Experimental characterization of stone masonry in shear and compression. Constr Build Mater 2009;23:3337–45. doi:10.1016/j.conbuildmat.2009.06.045.

[6] Lourenço PB, Oliveira D V., Roca P, Orduña A. Dry Joint Stone Masonry Walls Subjected to In-Plane Combined Loading. J Struct Eng 2005;131:1665–73. doi:10.1061/(asce)0733-9445(2005)131:11(1665).

[7] Vasconcelos G, Lourenço PB. In-Plane Experimental Behavior of Stone Masonry Walls under Cyclic Loading. J Struct Eng 2009;135:1269–77. doi:10.1061/(asce)st.1943-541x.0000053.

[8] Wang M, Liu K, Lu H, Shrestha H, Guragain R, Pan W, et al. Increasing the lateral capacity of dry joint flat-stone masonry structures using inexpensive retrofitting techniques. Bull Earthq Eng 2019;17:391–411. doi:10.1007/s10518-018-0454-1.

[9] Restrepo Vélez LF, Magenes G, Griffith MC. Dry Stone Masonry Walls in Bending—Part I: Static Tests. Int J Archit Herit 2014;8:1–28. doi:10.1080/15583058.2012.663059.

[10] Senthivel R, Lourenço PB. Finite element modelling of deformation characteristics of historical stone masonry shear walls. Eng Struct 2009;31:1930–43. doi:10.1016/j.engstruct.2009.02.046.

[11] Smoljanović H, Živaljić N, Nikolić Ž, Munjiza A. Numerical analysis of 3D dry-stone masonry structures by combined finite-discrete element method. Int J Solids Struct 2018;136–137:150–67. doi:10.1016/j.ijsolstr.2017.12.012.

[12] Smoljanović H, Živaljić N, Nikolić Ž. A combined finite-discrete element analysis of dry stone masonry structures. Eng Struct 2013;52:89–100. doi:10.1016/j.engstruct.2013.02.010.

[13] Chewe Ngapeya GG, Waldmann D, Scholzen F. Impact of the height imperfections of masonry blocks on the load bearing capacity of dry-stack masonry walls. Constr Build Mater 2018;165:898–913. doi:10.1016/j.conbuildmat.2017.12.183.

[14] Roca P. Assessment of masonry shear-walls by simple equilibrium models. Constr. Build. Mater., vol. 20, Elsevier; 2006, p. 229–38. doi:10.1016/j.conbuildmat.2005.08.023.

[15] Bui TT, Limam A, Sarhosis V, Hjiaj M. Discrete element modelling of the in-plane and out-of-plane behaviour of dry-joint masonry wall constructions. Eng Struct 2017;136:277–94. doi:10.1016/j.engstruct.2017.01.020.

[16] Pulatsu B, Erdogmus E, Bretas EM, Lourenço PB. In-Plane Static Response of Dry-Joint Masonry Arch-Pier Structures. AEI 2019, Reston, VA: American Society of Civil Engineers; 2019, p. 240–8. doi:10.1061/9780784482261.028.

[17] Chen X, Wang H, Chan AHC, Agrawal AK. Dynamic failure of dry-joint masonry arch structures modelled with the combined finite–discrete element method. Comput Part Mech 2020;7:1017–28. doi:10.1007/s40571-019-00297-2.

[18] Foti D, Vacca V, Facchini I. DEM modeling and experimental analysis of the static behavior of a dry-joints masonry cross vaults. Constr Build Mater 2018;170:111–20. doi:10.1016/j.conbuildmat.2018.02.202.

[19] Pulatsu B, Gencer F, Erdogmus E. Study of the effect of construction techniques on the seismic capacity of ancient dry-joint masonry towers through DEM. Eur J Environ Civ Eng 2020;0:1–18. doi:10.1080/19648189.2020.1824823.

[20] Erdogmus E, Pulatsu B, Can B, Ozkan K. Analysis of the Last Standing Arch of the Roman Aqueduct at Blaundos. In: Dillion PB, Fonseca FS, editors. 13th North Am. Mason. Conf., Salt Lake City: The Masonry Society; 2019, p. 483–93.

[21] Gonen S, Pulatsu B, Erdogmus E, Karaesmen E, Karaesmen E. Quasi-Static Nonlinear Seismic Assessment of a Fourth Century A.D. Roman Aqueduct in Istanbul, Turkey. Heritage 2021;4:401–21. doi:https://doi.org/10.3390/heritage4010025.

[22] Pulatsu B, Gonen S, Erdogmus E, Lourenço PB, Lemos J V., Hazzard J. Tensile Fracture Mechanism of Masonry Wallettes Parallel to Bed Joints: A Stochastic Discontinuum Analysis. Model Open Access J Model Eng Sci 2020;1:78–93. doi:10.3390/modelling1020006.

[23] Sarhosis V, Forgacs T, Lemos J V. Stochastic strength prediction of masonry structures: a methodological approach or a way forward? RILEM Tech Lett 2020;4:122–9. doi:10.21809/rilemtechlett.2019.100.

[24] Gonen S, Pulatsu B, Soyoz S, Erdogmus E. Stochastic discontinuum analysis of unreinforced masonry walls: Lateral capacity and performance assessments. Eng Struct 2021;238:112175. doi:10.1016/j.engstruct.2021.112175.

[25] Sarhosis V, Lemos J V. A detailed micro-modelling approach for the structural analysis of masonry assemblages. Comput Struct 2018;206:66–81. doi:10.1016/j.compstruc.2018.06.003.

[26] Pulatsu B, Kim S, Erdogmus E, Lourenço PB. Advanced analysis of masonry retaining walls using mixed discrete-continuum approach. Proc Inst Civ Eng - Geotech Eng 2020:1–34. doi:10.1680/jgeen.19.00225.

[27] Pulatsu B, Erdogmus E, Lourenço PB, Lemos J V., Tuncay K. Numerical modeling of the tension stiffening in reinforced concrete members via discontinuum models. Comput Part Mech 2020. doi:10.1007/s40571-020-00342-5.

[28] Lemos J V., Campos Costa A, Bretas EM. Assessment of the seismic capacity of stone masonry walls with block models. In: Papadrakakis M, Lagaros ND, Fragiadakis M, editors. Comput. Methods Earthq. Eng. Comput. Methods Appl. Sci., vol. 2, Springer; 2011, p. 584.

[29] Ravi Prakash P, Pulatsu B, Lourenço PB, Azenha M, Pereira JM. A meso-scale discrete element method framework to simulate thermo-mechanical failure of concrete subjected to elevated

temperatures. Eng Fract Mech 2020;239:107269. doi:10.1016/j.engfracmech.2020.107269.
[30] Pulatsu B, Erdogmus E, Lourenço PB. Simulation of Masonry Arch Bridges Using 3D Discrete Element Modeling. RILEM Bookseries, vol. 18, 2019, p. 871–80. doi:10.1007/978-3-319-99441-3_94.
[31] Pulatsu B, Erdogmus E, Lourenço PB. Comparison of in-plane and out-of-plane failure modes of masonry arch bridges using discontinuum analysis. Eng Struct 2019;178:24–36. doi:10.1016/j.engstruct.2018.10.016.
[32] Lourenço PB. Computations on historic masonry structures. Prog Struct Eng Mater 2002;4:301–19. doi:10.1002/pse.120.
[33] Roca P, Cervera M, Gariup G, Pela L. Structural analysis of masonry historical constructions. Classical and advanced approaches. Arch Comput Methods Eng 2010;17:299–325. doi:10.1007/s11831-010-9046-1.
[34] Itasca Consulting Group Inc. 3DEC Three Dimensional Distinct Element Code 2013.
[35] Cundall PA. The measurement and analysis of accelerations in rock slopes. University of London (Imperial College of Science and Technology), 1971.
[36] Pulatsu B, Bretas EM, Lourenço PB. Discrete element modeling of masonry structures: Validation and application. Earthquakes Struct 2016;11:563–82. doi:10.12989/eas.2016.11.4.563.
[37] Lemos J V. Discrete element modeling of the seismic behavior of stone masonry arches. In: G.N. P, Middleton J, Kralj B, editors. Comput. methods Struct. Mason., Florence: E&FN Spon; 1997, p. 220–7.
[38] Lemos J V. Discrete element modeling of masonry structures. Int J Archit Herit 2007;1:190–213. doi:10.1080/15583050601176868.
[39] Sarhosis V, Oliveira D V., Lemos J V., Lourenço PB. The effect of skew angle on the mechanical behaviour of masonry arches. Mech Res Commun 2014;61:53–9. doi:10.1016/j.mechrescom.2014.07.008.
[40] Malomo D, DeJong MJ, Penna A. Distinct element modelling of the in-plane cyclic response of URM walls subjected to shear-compression. Earthq Eng Struct Dyn 2019;48:1322–44. doi:10.1002/eqe.3178.
[41] Napolitano RK, Glisic B. Methodology for diagnosing crack patterns in masonry structures using photogrammetry and distinct element modeling. Eng Struct 2019;181:519–28. doi:10.1016/j.engstruct.2018.12.036.
[42] Pulatsu B, Sarhosis V, Bretas EM, Nikitas N, Lourenço PB. Non-linear static behaviour of ancient free-standing stone columns. Proc Inst Civ Eng - Struct Build 2017;170:406–18. doi:10.1680/jstbu.16.00071.
[43] Dimitri R, De Lorenzis L, Zavarise G. Numerical study on the dynamic behavior of masonry columns and arches on buttresses with the discrete element method. Eng Struct 2011;33:3172–88. doi:10.1016/j.engstruct.2011.08.018.
[44] Drei A, Milani G, Sincraian G. DEM numerical approach for masonry aqueducts in seismic zone: two valuable Portuguese examples. Int J Mason Res Innov 2017;2:1. doi:10.1504/IJMRI.2017.082392.
[45] Cundall PA. Distinct element models of rock and soil structure. In: Brown ET, editor. Anal. Comput. Methods Eng. Rock Mech., London: George Allen Unwin; 1987, p. 129–163.
[46] Pulatsu B, Erdogmus E, Lourenço PB, Lemos J V., Tuncay K. Simulation of the in-plane structural behavior of unreinforced masonry walls and buildings using DEM. Structures 2020;27:2274–87. doi:10.1016/j.istruc.2020.08.026.
[47] Pulatsu B, Erdogmus E, Lourenço PB, Quey R. Simulation of uniaxial tensile behavior of quasi-brittle materials using softening contact models in DEM. Int J Fract 2019;217:105–25. doi:10.1007/s10704-019-00373-x.

[48] Voyiadjis GZ, Kattan PI. On the decomposition of the damage variable in continuum damage mechanics. Acta Mech 2017;228:2499–517. doi:10.1007/s00707-017-1836-1.
[49] Oliveira D V. Experimental and numerical analysis of blocky masonry structures under cyclic loading. Universidade do Minho, 2003.
[50] Lotfi HR, Shing PB. Interface Model Applied to Fracture of Masonry Structures. J Struct Eng 1994;120:63–80. doi:10.1061/(ASCE)0733-9445(1994)120:1(63).
[51] Venzal V, Morel S, Parent T, Dubois F. Frictional Cohesive Zone Model for quasi-brittle fracture: Mixed-mode and coupling between cohesive and frictional behaviors. Int J Solids Struct 2020;198:17–30. doi:10.1016/j.ijsolstr.2020.04.023.
[52] Pulatsu B, Erdogmus E, Lourenço PB, Lemos J V., Hazzard J. Discontinuum analysis of the fracture mechanism in masonry prisms and wallettes via discrete element method. Meccanica 2020;55:505–23. doi:10.1007/s11012-020-01133-1.
[53] Gonen S, Soyoz S. Investigations on the elasticity modulus of stone masonry. Structures 2021;30:378–89. doi:10.1016/j.istruc.2021.01.035.
[54] Saloustros S, Pelà L, Contrafatto FR, Roca P, Petromichelakis I. Analytical Derivation of Seismic Fragility Curves for Historical Masonry Structures Based on Stochastic Analysis of Uncertain Material Parameters. Int J Archit Herit 2019;13:1142–64. doi:10.1080/15583058.2019.1638992.
[55] Milani G, Benasciutti D. Homogenized limit analysis of masonry structures with random input properties: polynomial Response Surface approximation and Monte Carlo simulations. Struct Eng Mech 2010;34:417–47. doi:10.12989/sem.2010.34.4.417.
[56] Park J, Towashiraporn P, Craig JI, Goodno BJ. Seismic fragility analysis of low-rise unreinforced masonry structures. Eng Struct 2009;31:125–37. doi:10.1016/j.engstruct.2008.07.021.
[57] Parisi F, Augenti N. Uncertainty in seismic capacity of masonry buildings. Buildings 2012;2:218–30. doi:10.3390/buildings2030218.
[58] Gönen S, Soyöz S. Reliability-based seismic performance of masonry arch bridges. Struct Infrastruct Eng 2021;0:1–16. doi:10.1080/15732479.2021.1918726.
[59] Gonen S. Reliability-based Seismic Assessment of Masonry Arch Bridges. Boğaziçi University, 2020.
[60] Pina-Henriques J, Lourenço PB. Masonry compression: A numerical investigation at the meso-level. Eng Comput (Swansea, Wales) 2006;23:382–407. doi:10.1108/02644400610661163.
[61] Boussabaine A, Kirkham R. Whole Life-Cycle Costing: Risk and Risk Responses | Wiley. Blackwell Publishing; 2004.
[62] Shields MD, Teferra K, Hapij A, Daddazio RP. Refined Stratified Sampling for efficient Monte Carlo based uncertainty quantification. Reliab Eng Syst Saf 2015;142:310–25. doi:10.1016/j.ress.2015.05.023.
[63] Olsson A, Sandberg G, Dahlblom O. On Latin hypercube sampling for structural reliability analysis. Struct Saf 2003;25:47–68. doi:10.1016/S0167-4730(02)00039-5.
[64] Calvi GM, Kingsley GR, Magenes G. Testing of masonry structures for seismic assessment. Earthq Spectra 1996;12:145–61.
[65] Tomazevic M. Some aspects of experimental testing of seismic behavior of masonry walls and models of masonry buildings. ISET J Earthq Technol 2000;37:101–17.
[66] TBDY. Türkiye Bina Deprem Yönetmeliği. 2018.
[67] ASCE/SEI 41-17. Seismic Evaluation and Retrofit of Existing Buildings. 2017.
[68] D'Ayala D, Ansal A. Non linear push over assessment of heritage buildings in Istanbul to define seismic risk. Bull Earthq Eng 2012;10:285–306. doi:10.1007/s10518-011-9311-1.
[69] Lagomarsino S, Cattari S. PERPETUATE guidelines for seismic performance-based assessment of cultural heritage masonry structures. Bull Earthq Eng 2015;13:13–47. doi:10.1007/s10518-014-9674-1.

Pre-print version: Pulatsu, B., Gonen, S., Erdogmus, E., Lourenço, P.B., Lemos, J.V., and Prakash R., "*In-Plane Structural Performance of Dry-Joint Stone Masonry Walls A Spatial and Non-Spatial Stochastic Discontinuum Analysis*.", Engineering Structures (2021). **DOI**: 10.1016/j.engstruct.2021.112620

[70] Kržan M, Gostič S, Cattari S, Bosiljkov V. Acquiring reference parameters of masonry for the structural performance analysis of historical buildings. Bull Earthq Eng 2015;13:203–36. doi:10.1007/s10518-014-9686-x.

[71] Vanin F, Zaganelli D, Penna A, Beyer K. Estimates for the stiffness, strength and drift capacity of stone masonry walls based on 123 quasi-static cyclic tests reported in the literature. Bull Earthq Eng 2017;15:5435–79. doi:10.1007/s10518-017-0188-5.

[72] Bosiljkov VZ, Totoev YZ, Nichols JM. Shear modulus and stiffness of brickwork masonry: An experimental perspective. Struct Eng Mech 2005;20:21–43. doi:10.12989/sem.2005.20.1.021.

[73] Bosiljkov V, Page AW, Bokan-Bosiljkov V, Žarnić R. Evaluation of the seismic performance of brick masonry walls. Struct Control Heal Monit 2010;17:100–18. doi:10.1002/stc.299.

View publication stats